MODIS Infrared Sea Surface Temperature Algorithm

Algorithm Theoretical Basis Document

Version 2.0

Submitted by

Otis B. Brown
Peter J. Minnett

With contributions from:
R. Evans, E. Kearns, K. Kilpatrick, A. Kumar, R. Sikorski & A. Závody

University of Miami
Miami, FL 33149-1098

April 30, 1999

Table of Contents

iv

Tables

Preface

This Algorithm Theoretical Basis Document (ATBD) describes our current working model of the algorithm for estimating bulk sea surface temperatures from the MODIS mid- and far-infrared bands. While effort has been made to make this document as complete as possible, it should be recognized that algorithm development is an evolving process. This document (V2.0) is a description of the prototype algorithm for MODIS sea surface temperature estimation as it currently exists, and has been delivered to NASA for inclusion in the MODIS processing scheme.

Current research on the physics of the atmospheric transmission in the infrared, of the processes at the ocean surface, and new information about the performance of the MODIS will lead to periodic revisions of the algorithms. Also, the document may appear incomplete in places as research continues to improve our understanding of the processes at work. Subsequent revisions of the document will reflect new knowledge and, it is hoped, fill the gaps in what is reported here.

The activities reported in this document are complimentary to other in the MODIS Ocean Team program, in particular those of Dr. R. H. Evans whose MODIS ATBD includes much of the implementation information needed for data flow and details of the operational computer codes.

The NOAA/AVHRR results described in this document are based on continuing joint development and tests associated with the NASA/NOAA Pathfinder AVHRR Oceans activity. Experience gained with the Pathfinder efforts is directly assisting development of the MODIS comparison database with respect to design, testing and implementation. Some of the pre-launch field activities discussed here include results of research cruises funded by the National Science Foundation and NASA Headquarters through research grants to PJM.

1.0 Introduction

The Earth Observing System (*EOS*) Moderate Resolution Imaging Spectrometer (*MODIS*) is a satellite based visible/infrared radiometer for the sensing of terrestrial and oceanic phenomena. The MODIS design builds on the heritage of several decades of NOAA infrared radiometer use [Schwalb, 1973; 1978]. An aspect of our efforts as members of the MODIS instrument team is to develop a state-of-the-art algorithm for the estimation of sea surface temperature (*SST*). The goal of this document is to describe the prototype pre-launch SST algorithm for the MODIS instrument, version1. Included in this description are physical aspects of the approach, calibration and validation needs, quality assurance, SST product definition and unresolved issues.

1.1   Algorithm and Product Identification

SST estimates produced by the proto-algorithm will be labeled version 1. This is a level 2 product with EOSdis product number 2527; it is MODIS product number 28, labeled Sea_sfc Temperature.

1.2   Algorithm Overview

This algorithm is being developed on the MODIS Ocean Team Computing Facility (*MOTCF*) for use in the EOS Data and Information System (*EOSdis)* core processing system and the Scientific Computing Facility at the Rosenstiel School of Marine and Atmospheric Science, University of Miami. The Sea_sfc Temperature determination is based on satellite infrared retrievals of ocean temperature, which are corrected for atmospheric absorption using combinations of several MODIS mid- and far-infrared bands. Cloud screening is based on two approaches: use of the cloud screening product (3660) and a cloud indicator derived during the SST retrieval. The latter approach consists of individual retrievals passing a series of negative threshold, spatial homogeneity, and delta-climatology tests. The quality assessment SST output products are vectors composed of the estimated SST value, input calibrated radiances and derived brightness temperatures for each band, flags which quantify the cloud screening results, scan coordinate information, latitude, longitude and time.   The

distributed Sea_sfc Temperature product consists of vectors composed of the SST estimate, latitude, longitude, time and quality assessment flags.

1.3   Document Scope

This document describes the physical basis for the Sea_sfc Temperature (SST) algorithm, gives the structure of the current version 1 algorithm, discusses implementation dependencies on other observing streams, and describes validation needs. The at-launch atmospheric correction algorithm is described and the anticipated error budget for the derived SST fields are discussed.

This replaces version 1.0, dated 21 October 1996. It differs from the earlier document by presenting the atmospheric correction algorithms in full, as well as giving a more detailed account of the validation plans, including the results of pre-launch research cruises. These have demonstrated the feasibility of validating the performance of the atmospheric correction algorithm using spectroradiometers at sea, and provided new insight into the physical processes at the ocean surface that are of prime relevance to the determination of the uncertainties in the MODIS SST retrievals.

1.4   Applicable Documents and Publications

MODIS SST Proposal, 1990, Infrared Algorithm Development for Ocean Observations with EOS/MODIS, Otis B. Brown

MODIS IR SST Execution Phase Proposal, 1991, Infrared Algorithm Development for Ocean Observations with EOS/MODIS, Otis B. Brown

2.0 Overview and Background Information

The importance of satellite-based measurements to study the global distribution and variability of sea surface temperature has been described in the MODIS Instrument Panel Report [MODIS, 1986] and elsewhere [ESSC, 1988; WOCE, 1985; Weller and Taylor, 1993], and will not be discussed here. Suffice it to say that global surface temperature fields are required on daily to weekly time scales at moderate resolution, *i.e.*, 10-200 km. Since the pioneering work of Anding and Kauth [1970] and Prabhakara *et al.,* [1974] it has been known that atmospheric water vapor absorption effects in the infrared can be corrected with high accuracy using linear combinations of multiple band measurements.   MODIS specifications ensure very low radiometer noise (<0.05K between 10 μm and 12 μm), as well as narrow, well placed windows in the 3.7μm to 4.2 μm band [Salomonson *et al.*, 1998]. These enhancements, together with new radiative transfer modeling tuned to the MODIS band selection, should permit global SST retrievals on space scales of ~10 km with RMS errors ≤0.45K for weekly fields at mid-latitudes with errors ≤0.5K in the tropics. Such fields are a necessary prerequisite to achieve the stated goal of accuracies at the 0.2K level for 2° x 2° squares [Weller and Taylor, 1993].

2.1   Experimental Objective

This algorithm development activity is part of a larger MODIS Instrument Team investigation to develop accurate methods for determination of ocean sea surface temperature, generate mapped SST fields, validate their characteristics, determine the principal modes of spatial and temporal variation for these fields, and develop a sequence of simple models to assimilate such fields to study specific scientific problems such as global warming. The proposed efforts will directly address the upper ocean mixed layer and permit computation of seasonally varying thermal fields to be used in both the Joint Global Ocean Flux Study (JGOFS)[GOFS, 1984] and World Ocean Circulation Experiment (WOCE)[WOCE, 1985] programs. These fields can be used to provide indices for ocean warming on seasonal to interannual scales and, thus, will directly address NASA Earth System Science objectives [ESSC, 1988]. Due to the complexity of the calibration, atmospheric correction, and data assimilation aspects of these fields, the overall effort requires close collaboration with other proposed EOS efforts with respect to the MODIS and ADEOS NSCAT measurement systems.

2.2   Historical Perspective

Development of algorithms for the production of reliable SST data sets from space borne infrared radiometers has been pursued by a number of investigators, agencies and governments since the late 1960's [see review by Brown and Cheney, 1983, and Abbott and Chelton, 1991, for details]. For example, NOAA [McClain, 1981; McClain *et al.*, 1983; Strong and McClain, 1984; McClain *et al.*, 1985], NASA [Shenk and Salomonson, 1972; Chahine, 1980; Susskind *et al.*, 1984], and RAL/UK [Llewellyn-Jones, *et al.*, 1984] address infrared radiometry, using a variety of radiation transfer codes, model and observed vertical distributions of temperature and moisture, and actual observations. Minnett [1986; 1990] and Barton [1995] summarize the present state of the art for high quality retrievals from NOAA AVHRR (Advanced Very High Resolution Radiometer) class instruments. The current state of the art is limited by radiometer window placement, radiometer noise, quality of pre-launch instrument characterization, in-flight calibration quality, viewing geometry, and the atmospheric correction.

2.3   Instrument Characteristics

MODIS has a number of infrared bands in the mid- and far-infrared which were placed to optimize their use for SST determination. Bands of particular utility to infrared SST determination are listed in Table 1.

Table 1. Bands for MODIS Infrared SST Determination

Band Number	Band Center (μ)	Bandwidth (μ)	NE•T (K)
20	3.750	0.1800	0.05
22	3.959	0.0594	0.07
23	4.050	0.0608	0.07
31	11.030	0.5000	0.05
32	12.020	0.5000	0.05

These bands were chosen for MODIS based on particular aspects of the atmospheric total column transmissivity in each part of the mid- and far-infrared spectrum. Figure 1 presents a profile of the expected earth radiance at satellite height from 3 μm to 14 μm.

The bands located near 4μm (20, 22, and 23) exhibit high sensitivity (defined as $\frac{1}{L}\frac{dL}{dT}$)
and are placed where the influence of column water vapor is minimal on the sensed
radiances. Bands in the far-infrared between 10μm and 12μm (31 and 32) are located
near the maximum emission for a 300K blackbody (an approximation for the average
Earth temperature) and placed such that there is a significant difference in the band
integrated water vapor absorption for the two bands. The mid-infrared bands, while
having minimal water vapor loading, suffer from decreased available Earth radiance,
narrow bandwidth and possible specularly reflected solar radiance during daylight.
The far-infrared bands are near the maximum of the Earth's emission and have larger
bandwidth, but are burdened by large water vapor absorption in the tropical air narrow
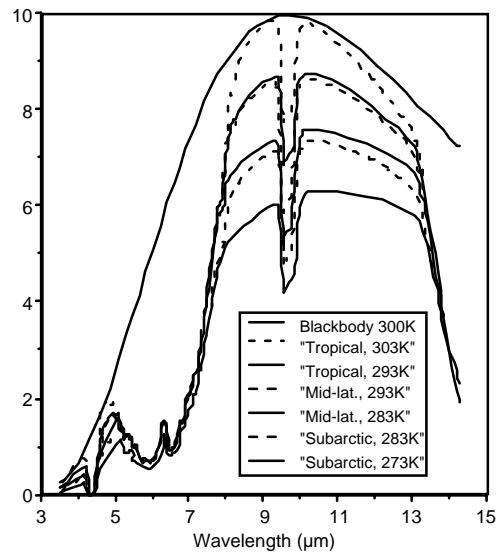
Figure 1. Earth radiance in the mid- to far-infrared spectrum. The various
curves give a range of expected infrared radiances for a variety of typical
atmospheres and surface temperatures. A 300K blackbody curve is provided
to permit visual comparison of the path length absorption for the various
cases. Profile data is computed by the Lowtran radiative transfer program
[Selby *et al.*, 1978].

bandwidth and possible specularly reflected solar radiance during daylight. The far-
infrared bands are near the maximum of the Earth's emission and have larger
bandwidth, but are burdened by large water vapor absorption in the tropical air
masses. The mid- and far-infrared bands differing sensitivity to total column water
vapor complement each other and provide a balanced infrared SST observing strategy.
The specified NEΔT for each band is ≤0.07K. As will be seen, these characteristics are
necessary prerequisites for accurate SST determination at the desired level of accuracy.

5

3.0 Algorithm Description

This section describes the proto-MODIS infrared algorithm. It includes a theoretical overview, a physical basis for the approach, and several sub-sections which discuss implementation and accuracy issues.

3.1   Theoretical Description

Given well-calibrated radiances from MODIS, deriving accurate sea surface temperature fields and associated statistics is dependent on one's abilities to correct for the effects of the intervening atmosphere on these spectral radiances and to provide assimilation mechanisms which cover the time-space windows of interest. Sensing SST through the atmosphere in the thermal infrared is subject to several environmental factors that degrade the accuracy of the perceived temperature. Major sources of error in the radiometric determination are (a) sun glint (MODIS bands 20, 22, and 23), (b) water vapor absorption in the atmosphere (MODIS bands 31, 32), (c) trace gas absorption (all bands) and (d) episodic variations in aerosol absorption due to volcanic eruptions, terragenous dust blown out to sea, etc. (all bands). Although satellite radiometers sense the ocean's radiation temperature known as "skin" temperature, satellite results are commonly compared with bulk temperature measurements in the upper several meters of the ocean. Air-sea interaction modifies the relationship between these two variables and causes observable differences in the bulk and radiation temperatures [Robinson, *et al.*, 1984; Cornillon and Stramma, 1985; Schluessel *et al.*, 1990]. We must be prepared to quantify regional and temporal differences between bulk and skin temperatures. This is one of the goals of the *in situ* SST calibration and validation activity.

The integrated atmospheric transmissivity over each of the MODIS infrared bands (20, 22, 23, 31, and 32) differs. Consequently, algorithms can be constructed which depend on the differences in measured temperature among these bands [Anding and Kauth, 1970]. The simplest such algorithm assumes that, for small cumulative amounts of water vapor, the atmosphere is sufficiently optically thin that the difference between the measured temperature in any band and the true surface temperature can be parmeterized as a simple function of the difference between the measured temperatures in two bands with different atmospheric transmissions.

6

We are using the line-by-line numerical radiative transfer code developed at Rutherford Appleton Laboratory in the UK as a basis for modeling atmospheric absorption and emission processes in the MODIS infrared bands: [Llewellyn-Jones, *et al.*, 1984; Závody , *et al.*, 1995]

Linear algorithms (MCSST) are based on a formula of the following form for the surface temperature T_s:

$$T_s = \alpha + \beta \, T_i + \gamma (T_i - T_j) \qquad (1)$$

where the T_i's are brightness temperatures in various bands for a given location and the coefficients α, β and γ give the parameterized correction [Deschamps and Phulpin, 1980; Llewellyn-Jones *et al.*, 1984], or can be derived empirically from good composite sets of surface and satellite observations [Prabhakara, *et al.*, 1974]. In Eq. (1) such an algorithm constructed on bands 31 and 32 would replace *i,j* by 31, 32 respectively. Equivalent relations can be constructed for any two band pairs. α, β and γ values are -1, 1, and 3, respectively, for a typical AVHRR 4,5 algorithm (T_s in °C) [McClain *et al.*, 1983].

Although Eq. (1) is easy to implement, it does not permit correction for changes in air mass due to scan-angle. Llewellyn-Jones *et al.*, [1984] develop a table from numerical simulations which permits modification of Eq. (1) into a form:

$$T_s = \alpha + \beta' \, T_i + \gamma' (T_i - T_j) + \delta \, (1 - \sec(\theta)) \qquad (2)$$

where θ is the zenith angle and δ is an additional scan angle coefficient. This approach reduces the errors at large scan angles for moist atmospheres by more than 1K.

For MODIS Sea_sfc Temperature estimation (proto-algorithm) we will eventually implement a correction equation which is a variation of Eq. (2) for multiple pairs of the available bands (see Section 3.1.1). This will be coupled with an objective criterion based on observed retrieval scatter for a local region determine which band combination(s) is (are) used.   We will also examine the possibility of implementing a version of NLSST technique [Walton *et al.*, 1990] which provides a nonlinear approach to atmospheric correction.

3.1.1 Physics of the Problem

It has been noted that satellite infrared radiances can be straightforwardly corrected for atmospheric absorption in the water vapor bands by utilizing a split (or dual) window technique. In this and the following discussions we will assume that bands are chosen such that water vapor is the primary variable absorbing gas, O_3 variation is minimal, the column is cloud free, and specularly reflected sunlight is not present. We outline a theoretical basis for the split or dual window methods. Split and dual window refer to use of two bands in the 10µm-12µm band (split) or to two bands in the 4µm and 10µm-12µm bands (dual) and follows Deschamps and Phulpin [1980]. This derivation is for a nadir view through an atmosphere, which can be characterized by species invariant, vertically integrated absorbents. In practice it has been shown that this simplification of the problem will address scan angles within 30° of the nadir and all but the most moist tropical atmospheres (see Fig. 2a).

It is easily shown that, for a non-scattering atmosphere, the outgoing infrared radiance at the top of the atmosphere in the mid- and far-infrared, normal to the earth, can be represented by:

$$L_\lambda = L_\lambda \,(Surface) t_\lambda \,(O,P_o) - \int_o^{P_o} B_\lambda [T(P)] dt_\lambda \,(O,P), \qquad (3)$$

where L_λ is the radiance, $t_\lambda (0,P_x)$ the transmissivity from a pressure level P_x to the top of the atmosphere, and B_λ (T) the Planck function. This neglects the small contribution of energy emitted by the atmosphere downwards, and reflected into the upwelling beam at the sea surface. Following Deschamps and Phulpin [1980] this can be written as:

$$\Delta L_\lambda = B_\lambda \,(T_o) - L_\lambda \qquad (4)$$

$$= \int_o^{P_o} [B_\lambda \,(T_o) - B_\lambda \,(T(P))] \; dt_\lambda \,(O,P) \qquad (5)$$

i.e., ΔL_λ is the radiance error introduced by the atmosphere. Equivalently we can write this as a temperature deficit:

$$\Delta T_\lambda \;=\; T_o - T_\lambda \qquad (6)$$

8

Relating the temperature T_λ to the radiance $L_\lambda (T)$ by the Planck function we find:

$$\Delta T_\lambda = \frac{\Delta L_\lambda}{(\partial B / \partial T)\big|_{T_o}} \tag{7}$$

For an optically thin gas the following approximations can be made:

$$dt_\lambda (O,P) \cong - k_\lambda \, dU(P) \tag{8}$$

where k_λ is the absorption coefficient at wavelength, λ, and $U(P)$ is the optical path-length of the gas from the top of the atmosphere to pressure level P.

Secondly, we assume that the Planck function is adequately represented by a first order Taylor series expansion in each band window, *i.e.*,

$$B_\lambda [T(P)] = B_\lambda (T_o) + \left(\frac{\partial B_\lambda}{\partial T} \right) \Big|_{T_o} [T(P) - T_o] \tag{9}$$

Upon substitution of (7), (8) and (9) into (5) we see

$$\Delta T = k_\lambda \int_o^{P_o} [T_o - T(P)] \, dU(P), \tag{10}$$

that is, the error is partitioned into a strict function of k_λ and a wavelength independent integral over atmospheric parameters. Thus, if one picks two spectral regions of the atmosphere, one has two linear equations with different k_λ 's to solve simultaneously.

For a two band system we can represent the SST as

$$T_S \; = \; a_o \, + \, a_1 \, T_1 + a_2 \, T_2 \tag{11}$$

with a_0 being included as an overall adjustment for wavelength independent attenuation. The constants a_1 and a_2 are determined theoretically, as above, or empirically, and are dependent on the optical absorption in the two radiometer bands. This is a simple transformation of Eq. (1) with $a_0 = \alpha$, $a_1 = \beta + \gamma$, and $a_2 = -\gamma$.

Such linear algorithms have been used for the split and dual windows between 10 μm and 12 μm bands [McClain *et al.*, 1983, 1985, and others]. Various workers have shown that it is difficult to have the best performance in a specific locale with a globally tuned

9

algorithm, *i.e.,* an algorithm that has been tuned over a large number of atmospheric states does not show optimum performance in a regional study [*e.g.,* Minnett, 1990]. It is apparent from the derivation that this is due to the assumptions about the vertical distribution of water vapor and the invariance of k_λ. In practice, one finds that the largest outliers are for extreme temperature, humidity, or scan angle situations.

Figure 2a shows departures from linearity between *in situ* surface bulk temperatures and space derived sea surface temperatures based on a linear algorithm such as Eq. 11. It is readily seen that the major departures from linearity are at high temperatures and high scan angles.
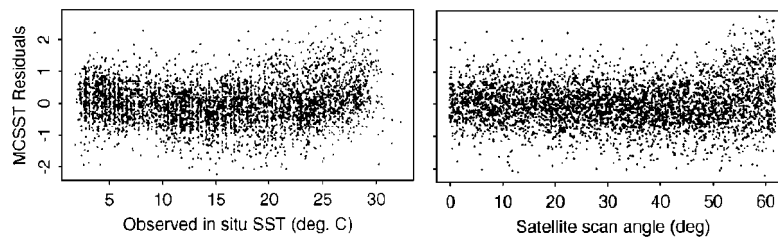
Figure 2. Comparison of MCSST SST estimates with fixed buoy observations taken from the AVHRR analog of the "North American" matchup database. MCSST coefficients a_0 = -0.0024, a_1 = 3.53, a_2 = -2.52. RMS difference of the ensemble is 0.66K. Figure 2a. Residual *vs. in situ* temperature. Figure 2b. Residual *vs.* satellite scan angle.

For temperature residuals shown in Fig. 2a, the envelope shows greater span and positive residual bias for temperatures greater than 25°C. While the dependence on scan angle in Fig. 2b is minimal for angles less than 50°, there is a dramatic expansion of the envelope and a positive trend apparent for larger angles. The two aspects of the MCSST algorithms displayed in Fig. 2 are the principal reason for examining other algorithms with improved high temperature, large air mass characteristics. The angular dependence of the residuals results from the inherent non-linearity of the radiative transfer process, the emission-angle dependence of the surface emissivity, neglected in the linear algorithm derivation, and the reflection of downwelling sky radiation.

While there have been a number of different methods employed to address this problem, the simplest approach currently available is to characterize the large air mass, *i.e.,* absorption cases, by adding a constant multiplying an angular function to the SST estimator. The correction equation in Eq. 2 is an example of this approach. In general, for a two-band system, one uses an estimator of the form:

$$T_S = a_0 + a_1 T_1 + a_2 T_2 + a_3 f(\theta) \tag{12}$$

where $f(\theta)$ is some appropriately chosen function of scan or zenith angle. This form, however, while improving the error behavior at large scan angles, does not adequately control the residual behavior at high temperatures.

A further generalization of this approach is to posit a non-linear structure for the SST estimator. As a starting point for this investigation, we define a NLSST (non-linear SST) atmospheric equation following Walton [1990]. The NLSST algorithm is a derivative of the CPSST (cross-product SST) algorithm [Walton, 1988] and forms the basis of the current operational AVHRR SST retrievals. Our working definition uses the form:

$$T_S = a_0' + a_1' \, T_1 \ + \ a_2' \, (T_1 - T_2) \cdot T_b \ + \ a_3' \, (\sec \theta - 1) \tag{13}$$

where the terms T_S, and T_i are as defined in Eq. 12, and T_b is the environmental temperature. While Eq. 13 can be viewed as a generalization of Eq. 12, there is a notable departure from the MCSST form. The inclusion of an environmental temperature, T_b , as a multiplier for a brightness temperature difference between the two bands provides a different behavior at higher temperatures.

Figs. 3a and 3b present the results of a matchup comparison with fixed buoy data off the US East Coast using Eq. 12 as the SST estimator. The improvement in behavior at both high temperatures and large air masses is apparent. For the matchup data set considered this approach provides an improvement of about 20%, or 0.13K in the error residual. A problem with implementing this version of the algorithm is the T_b term. One must have a estimate of the temperature for the pixel within $\pm \ 2\sigma$ prior to estimating its value. Typically this is done using a climatology or an MCSST type algorithm as a first guess.

Eq. 13 will be the form of the delivered proto-algorithm. That is, we will furnish the coefficients and $f(\theta)$ computed to retrieve an optimal Sea_sfc Temperature for combinations of bands, two at a time. We expect this algorithm to improve based on sufficient iteration between model and *in situ* validation results. Current testing with AVHRR SST retrievals suggests that Eq. 13 for two bands placed in the 10 μm to 12 μm window can provide estimates of SST with RMS errors below the 0.5K-0.6K level.
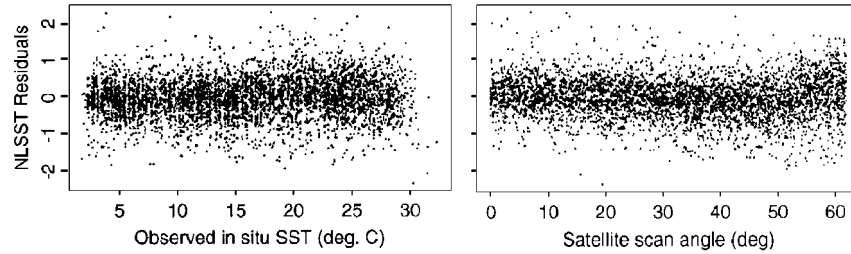
Figure 3. NLSST atmospheric correction algorithm comparison with *in situ* buoy data based on the AVHRR analog of the "North American" matchup database. NLSST coefficients are $a_0' = 1.42$, $a_1' = 0.94$, $a_2' = 0.098$ and $a_3' = 0.88$. The RMS of the difference ensemble is 0.53C. Fig. 3a. Residuals *vs. in situ* temperature. Fig. 3b. Residuals *vs.* satellite scan angle.

Experience with the AVHRR Ocean Pathfinder data has shown that to achieve these levels of accuracy it is necessary to use time-dependent coefficients in the NLSST algorithm. These are slowly varying, being weighted means over a three-month interval.

Details of the AVHRR Ocean Pathfinder Matchup Database [Podestá *et al.*, 1996] can be found on the WWW at URL http://www.rsmas.miami.edu/~gui/matchups.html. Development work planned (and proposed) over the next several years will enhance this SST estimation equation in several ways. First, by using the new MODIS bands around 4 μm we will implement a set of split window algorithms which should work markedly better in very moist, tropical atmospheres. Second, we will explore the use of higher order nonlinear algorithms. Third, as the calibration-validation database coverage is enlarged, we will develop a parallel set of SST skin temperature algorithms based on this formalism.

3.1.2 Mathematical Aspects of the Algorithm

Implementation of this algorithm is straightforward. There are no particular mathematical issues, which must be resolved for successful implementation of the current algorithm.

3.1.3 Variance or Uncertainty Estimates

The uncertainty in the MODIS IR SST retrieval is straightforward to calculate. Taking Eq. 11 and performing an error analysis, one sees that the error in T_s can be represented as:

$$e_t = \sqrt{\sum_{i=1}^{n} a_i e_i^2} \qquad (14)$$

where e_t is the total error, a_i are the estimation coefficients, and e_i is the error apparent for each band i used in the algorithm. e_i is given by

$$e_i = \sqrt{\left(e_i^a\right)^2 + (NE\Delta T_i)^2} \qquad (15)$$

with e_i^a being the error due to atmospheric correction and $NE \cdot T_i$ deriving from instrumental design and performance considerations. Since the constants a_i are order 1, and one assumes that the nadir and/or atmospheric errors are comparable and the various bands have similar characteristics, one can see the error scales as

$$e_t = \sqrt{n}\, e_i \qquad (16)$$

where n is the number of bands used.

This analysis makes clear the fact that calibration and/or atmosphere correction errors are important components of the error budget, *i.e.*, 0.1K of error in calibration for a band is effectively an rms error in a dual band algorithm of 0.14K, assuming perfect atmospheric correction. Therefore, we have requested that the calibration be demonstrably accurate at the choice of 0.05K level to minimize the effect of calibration errors. The best atmospheric correction currently available for ATSR suggests that errors due to atmospheric correction in optimal cases for a nadir viewing instrument are approximately 0.3K [Mutlow, *et al.*, 1994; Minnett, 1990; Barton, *et al.*, 1993; Minnett, 1995b].

If one assumes that the calibration errors and the atmospheric errors are random and thus can be RSS'd, as in the preceding analysis, one sees that expected errors of 0.35K-

0.4K in the result are the best that can be expected for two-band configurations. This equation also points out that there is a cost associated with adding more bands to improve atmospheric correction. In addition to providing information potentially useful for correcting the effects of the intervening atmosphere, each additional band also introduces noise into the SST retrieval.

3.2   At-launch Atmospheric Correction Algorithms

In this section we describe the derivation of the at-launch algorithm for the retrieval of SST from the calibrated radiances measured in the appropriate MODIS bands. Because the algorithm has to be in place at the time the first measurements are transmitted from the satellite, its derivation must be based on experience gained from analysis of the measurements from heritage instruments, and on numerical modeling of the physics of the measurement. There are three components to the numerical simulations of the MODIS measurements and these are

- processes at the ocean surface that control the infrared emission,
- processes in the atmosphere that modify the infrared radiation between the surface and the aperture of the instrument, and
- effects of the instrument characteristics that introduce uncertainties into the measurements.

The emissivity of the sea-surface is high in the infrared spectral intervals of concern, and relatively invariant under the usual range of environmental conditions. As a result, variability in the surface processes is not a major source of uncertainty in the MODIS measurement. Variation of the surface emissivity as a function of emission angle (or, equivalently, scan angle or satellite zenith angle) is treated explicitly in the numerical simulations, but the effects of wind speed and surface cleanliness are not. The tilting of facets of the sea surface by the wind [Cox and Munk, 1954] induces an apparent wind-speed dependency of the emissivity and therefore also the reflectivity. Recent modeling results [Watts *et al*, 1996, Wu and Smith, 1997] imply that the wind-speed dependence to be much smaller than indicated in earlier studies [Masuda *et al.*, 1988], and to be small for emission angles less than 60°. Thus the wind-speed dependence of the sea-surface emissivity over the emission angles encompassed by the MODIS swath are relegated to secondary importance.

The modeling effort is therefore concentrated on the effects of the intervening atmosphere. Clouds, of course, are an effective barrier to the propagation of the surface-emitted radiation and are excluded from the simulations, it being assumed that MODIS pixels contaminated by cloud effects will be identified and removed from the SST derivation procedure. The simulations are restricted to cloud-free conditions, but experience with AVHRR and ATSR data [Edwards *et al.*, 1990; Minnett, 1995a & 1995b] indicates that aerosols are a significant error source. Some initial results of aerosol effects are presented below.

The modeling described here does not include the propagation of the radiation through the instrument to the detectors. The simulations are for the spectra of the emergent infrared radiation at the "top of the atmosphere" at satellite height. Models of the instrumental effects have been developed by the MCST and the results of these are used here in the construction of the SST retrieval error budget.

3.2.1 Numerical modeling

The atmospheric radiative transfer model used to simulate the top of atmosphere radiance was developed at Rutherford Appleton Laboratory (RAL) in the UK for the pre-launch prediction of the performance of the ATSR and the derivation of the atmospheric correction algorithm [Závody *et al.*, 1995]. It was first validated by use with data from the AVHRR on NOAA-7 [Llewellyn-Jones *et al.*, 1984], in that a set of atmospheric correction algorithms derived using the model produced SST fields of an accuracy comparable to that of the NOAA SST product, which was generated using an algorithm derived from match-ups with drifting buoys [Strong and McClain, 1984].

The model is a high spectral resolution line-by-line model that treats explicitly the three components of radiance in the field of view of the radiometer – the surface emission, emission from the atmosphere into the field of view, and downwelling atmospheric emission that is reflected into the beam at the sea surface. The spectral resolution of the model is 0.04 cm^{-1} and the atmosphere is treated as a comprising 128 uniform plane parallel layers distributed in equal pressure intervals. The spectral characteristics of each absorption line (spectral position, line strength, temperature dependence and pressure broadening coefficient) are taken form the HITRAN database [Rothman *et al.*, 1987]. As the model steps through the spectrum all lines are considered within 20 cm^{-1} of their line center, with the line shape being given by the Gross [1955] approximation.

15

The atmospheric constituents considered are ozone (O_3), nitrogen (N_2), nitric acid (HNO_3), nitrous oxide (N_2O), ammonia (NH_3), methane (CH_4), carbonyl sulfide (OCS) and the freons F11 (CCl_3F) and F12 (CCl_2F_2) which are treated as well-mixed gases at concentrations taken from the literature [see Závody *et al.*, 1995]; and water vapor (H_2O). Water vapor is treated in terms of both individual spectral lines, and the anomalous absorption continuum, which is described using the recent formulation of Clough *et al.* [1989; Mlawer *et al.* 1998]. The spatial and temporal variations in atmospheric water vapor concentrations require that realistic distributions be used in the simulations, and these are provided here in two forms: as a regionally and seasonally diverse set of marine atmosphere profiles derived from radiosonde ascents, and as a set of profiles produced by the global assimilation model of the European Center for Medium-Range Weather Forecasting (ECMWF). These data sets also provide the associated distributions of the atmospheric temperature and pressure profiles.

The model formulation allows the insertion of aerosol layers in the atmosphere, as these are believed to have a profound influence on the propagation of the infrared radiation. However, there are large uncertainties associated with the specification of the spectral properties, size, spatial and temporal distributions of aerosols and the inclusion of aerosols to provide realistic simulations is a subject of continuing research (see below). For the derivation of the at-launch SST retrieval algorithm, the atmosphere has been aerosol-free, it being presumed that the cloud-screening procedures implemented in the SST derivation will identify optically thick aerosol layers as clouds, and that the aerosol products derived by the MODIS Atmosphere Group (MOD04 – Kaufman and Tanré) will provide further indications of when aerosol effects might contaminate the SST retrievals.

Simulations across the MODIS swath are accomplished by scaling the atmospheric layer thickness by the secant of the satellite zenith angle (θ).

The output from the model is a set of spectra of atmospheric transmission, $\tau(\lambda,\theta)$, and upward atmospheric emission at the top, $L{\uparrow}(\lambda,\theta)$, and downward atmospheric emission at the bottom, $L{\downarrow}(\lambda,\theta)$, of the atmosphere. These are used with the spectrum of emission, $L_s(\lambda, SST)$, from the sea-surface and the surface emissivity, $\varepsilon(\lambda,\theta)$, to produce the spectrum of radiance emerging at the top of the atmosphere, $L_{toa}(\lambda,\theta)$:

$$L_{toa}(\lambda,\theta) = (\varepsilon(\lambda,\theta) \, L_s(\lambda, SST) + (1-\varepsilon(\lambda,\theta)) \, L{\downarrow}(\lambda,\theta))\tau(\lambda,\theta) + L{\uparrow}(\lambda,\theta) \qquad (17)$$

where the SST is given by a selected air-sea temperature difference referenced to the surface level air temperature of the atmospheric profile. $L_{toa}(\lambda,\theta)$ is combined with the normalized system-level response function $\varphi_i(\lambda)$ for band *i* to produce the simulated radiance measurement under the conditions prescribed by the model input.[1]

Further details of the model, and previous applications, are available in Llewellyn-Jones *et al.*, [1984], Minnett [1986, 1990], and Závody *et al.*, [1995].

3.2.2. Thermal infrared algorithm (10 -12 μm)

In this section we describe the application of the RAL model to derive the at-launch atmospheric correction algorithm using two distinct sets of atmospheric profiles. The resulting coefficients are reassuringly similar.

3.2.2.1 Radiosonde based

The RAL radiative transfer model was used with a global dataset of 1200 quality-controlled radiosondes at 5 zenith angles and 5 air-sea temperature differences to generate a database of 30000 brightness temperatures in each of MODIS bands 31 and 32. The basis for the MODIS V.2 pre-launch SST algorithm is the Miami Pathfinder SST (mpfsst) algorithm, developed at UM-RSMAS, which is:

$$\text{modis\_sst} = c_1 + c_2 * T_{31} + c_3 * T_{3132} + c_4 *(\sec(\theta) -1) * T_{3132} \tag{18}$$

T_{30} is the band 31 brightness temperature (BT) (*cf.* AVHRR Channel 4)
T_{3132} is (Band32 - Band31) BT difference (*cf.* AVHRR (Channel 4 - Channel 5))
θ is the satellite zenith angle

The algorithm differentiates atmospheric vapor load using the difference between the brightness temperatures (T_{3132}) for the 11 and 12 μm bands (MODIS bands 31 and 32).

---

[1] It is recognized that each of the 10 channels within each MODIS band has an individual $\varphi_i(\lambda)$ caused by the slightly differing optical paths through the instrument, and by the detector properties. An initial investigation of the differences in each channel indicates that these may make a noticeable contribution to the SST error budget, which could be corrected by channel-specific coefficients in the atmospheric correction algorithm. This is the subject of continuing research. For the algorithms presented here a band-averaged $\varphi_i(\lambda)$ has been used

Coefficients are determined for T_{3132} greater or less than 0.7K. In application, the coefficients are then weighted by measured T_{3132}.

The 30000-point database was run through a robust regression to fit the modis_sst. Data are weighted according to the residuals, discarding data more than one Standard Deviation from the basic regression. A subsequent regression derives the coefficients (Table 2). Residuals of that regression increased notably for Arctic and Antarctic terrestrial stations with surface temperatures below -2°C, which would be unrealistic for marine atmospheres. Excluding those extremely cold data, the series of regressions were re-run. The MODIS V.2 pre-launch modis_sst has a predicted RMS error of 0.337K about zero mean error.

Table 2. Coefficients for the MODIS Band 31 and 32 SST retrieval algorithm, derived using radiosondes to define atmospheric properties and variability.

	Coefficients	
	$T_{30} - T_{31} <= 0.7$	$T_{30} - T_{31} > 0.7$
c_1	1.228552	1.692521
c_2	0.9576555	0.9558419
c_3	0.1182196	0.0873754
c_4	1.774631	1.199584

While the radiosonde database was somewhat biased toward warmer SST's (figure 4) and clearer atmospheres, this bias was reduced by the statistics-based rejection of outliers. The plot of modeled band 31 *vs* band 32 resembles the distribution of previously collected Pathfinder data (figures 5 and 6). Residuals showed no major trend *vs* zenith angle or SST (figure 7), but are greater at high latitudes (figure 8).
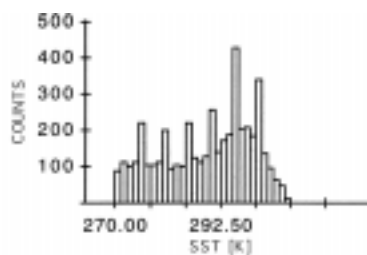
Figure 4. The modeled brightness-temperature database, filtered to remove surface temperatures below -2°C, is show fairly uniform distribution versus surface temperature.
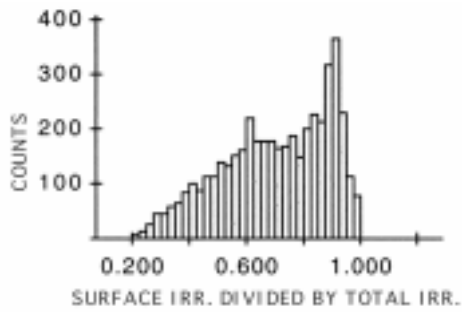
Figure 5. The distribution of atmospheric clarity, represented as fraction of surface-leaving radiance divided by total satellite-viewed radiance in band 31, in the modeled brightness-temperature database, filtered to remove surface temperatures below -2°C.
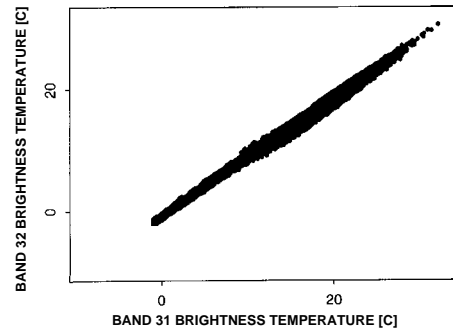
Figure 6. Modeled brightness-temperatures for band 31 *vs* band 32 shows a spreading of values above 15°C, which is also typical of Pathfinder data.
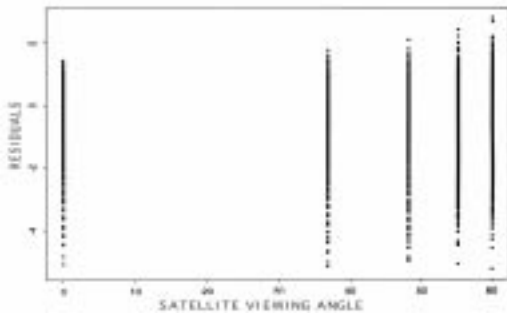
Figure 7. Residuals from the least-squares regression for the MODIS V.2 pre-launch algorithm show a small trend versus satellite zenith angle. (Surface temperatures > -2°C)
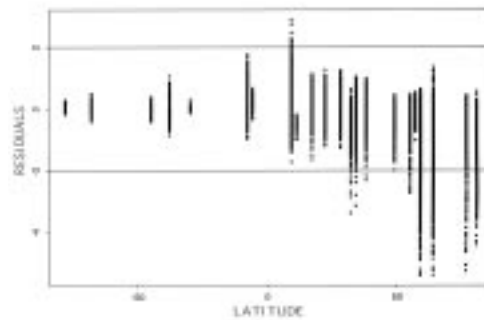
Figure 8. Residuals from the least-squares regression for the MODIS V.2 pre-launch algorithm are greatest at high latitudes. (Surface temperatures > -2°C)

$T_{3132} < 0.7°C$

$T_{3132} > 0.7°C$
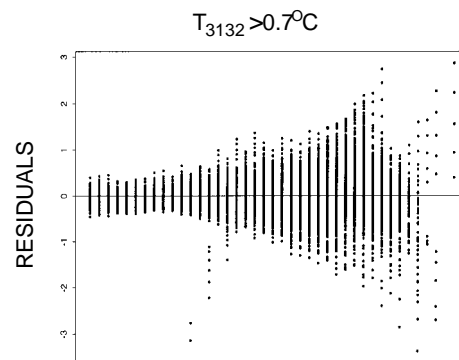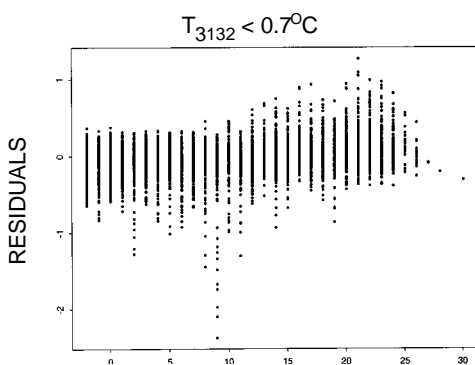
Figure 9. Residuals from the least-squares regression fit for the MODIS V.2 pre-launch algorithm show no major trends versus SST, with T_{3132} greater or less than 0.7°C. (Surface temperatures > -2°C)

19

3.2.2.2. ECMWF based

Subsequent to the derivation of the coefficients above, a new data set of atmospheric conditions became available. This is based on the output of the ECMWF assimilation model. These are 'pseudo-sondes' uniformly distributed at 10° latitude and longitude intervals. They were extracted from the ECMWF Global Data Assimilation Model at 00 and 12 UTC on the 1st and 16th of each every second month (January, March,…) of 1996. These have the advantage of uniformly representing the global range of marine atmospheric conditions. Provided they faithfully statistically represent the real atmosphere, they should lead to a set of coefficients that give SST fields with smaller uncertainties than those derived above from a radiosonde set that may not sample the whole atmospheric parameter space [Minnett, 1990].

The set of 2790 ECMWF pseudo-sondes were used with the model at eight zenith angles (0° to 60°, *i.e.* one to two air masses), and five sea-air differences (-0.5 to 1.5 K). The resulting coefficients are given in Table 3. Because of their more representative nature, and the fact that they do not differ markedly in values and characteristics to those derived from real radiosoundings, the coefficients derived from the ECMWF profiles form the basis of the MODIS at-launch SST atmospheric correction algorithm.

Table 3 Coefficients for the MODIS Band 31 and 32 SST retrieval algorithm, derived using ECMWF assimilation model marine atmospheres to define atmospheric properties and variability.

	Coefficients	
	$T_{30} - T_{31} <= 0.7$	$T_{30} - T_{31} > 0.7$
c_1	1.11071	1.196099
c_2	0.9586865	0.9888366
c_3	0.1741229	0.1300626
c_4	1.876752	1.627125

The predicted rms uncertainty in the SST retrievals is 0.345K, which is marginally larger than the value for the coefficients derived from the radiosondes. This is believed to result from the fact that the new set represents a wider range of atmospheric conditions.

As with the earlier set the uncertainties increase with increasing zenith angle. This is to be expected, but further effort will be invested in attempting to reduce the zenith angle dependence.

3.2.3. Mid-range infrared algorithm (3.7 – 4.2 μm)

The MODIS is the first spacecraft radiometer to have several infrared bands in the 3.7-4.1μm atmospheric window with characteristics suitable for the derivation of SST. This window is more transparent than that at 10-12 μm (bands 31 and 32) and provides the opportunity to derive more accurate SST fields. Although the heritage instruments have had single channels in this window, the data from which have been used in conjunction with those from the longer wavelength window to derive SST [*e.g.* Llewellyn-Jones *et al.*, 1984], MODIS provides the first opportunity to derive SST using measurements in this window alone. In developing the atmospheric correction algorithm for these bands we began with the simplest linear formulation (see 3.1 above) and introduced additional terms to reduce the residual uncertainties. In the initial phase simulations were done for a zenith angle of 0°, as the zenith angle dependency can be subsequently accommodated with a term involving a function of *sec (θ).*

The main disadvantage of this spectral interval for SST measurements is the contamination of the oceanic signal by reflected solar radiation in the daytime. Because of the wind roughening of the sea surface the reflection of the insolation becomes spread out over a large area when viewed from space – the sun-glitter pattern [*e.g.* Cox and Munk, 1954]. This can render a large fraction of the daytime swath unusable for SST determination. As a consequence, algorithms using measurements in this interval have been restricted to night-time use, or to those parts of the daytime swath where the risk of solar contamination can be confidently discounted. Thus, while the MODIS bands 20, 22 and 23 offer radiometric advantage over bands 31 and 32, they cannot offer the day and night applicability of the longer wavelength bands.

The RAL model was used first with a global dataset of 761 marine and coastal radiosondes to simulate satellite-viewed brightness temperatures (BTs) for the currently available response functions for MODIS AM-1 bands 20, 22 and 23. (Band 21 is also in this atmospheric window but because it has an extended dynamic range designed for the measurement of forest fires it does not have the radiometric sensitivity necessary for SST determination).

Table 4. MODIS response functions for bands 20, 22 and 23

Band	Center width (nm)	Bandwidth (nm) From 1% to 1%
20	3788.2	182.6
22	3971.9	88.2
23	4056.7	87.8

The simplest atmospheric correction algorithm is a linear function of a single band. This has a prospect of being effective if the band is in a very clear spectral interval that is largely unaffected by water vapor. The algorithm is:

$$SST_i = a_i + b_i * T_i \qquad (19)$$

where *i* is the band number.

The coefficients and residual SST errors are given in table 5, which demonstrates the capabilities of these clear spectral intervals, especially band 22.

Table 5. Coefficients and residual SST errors of linear single band atmospheric correction algorithm.

Band	a_j	b_j	$\varepsilon(SST)$
20	1.01342	1.04948	0.320
22	1.64547	1.02302	0.170
23	3.65264	1.04657	0.446

The residual errors can be reduced still further by a combination of two channels. The simple multichannel SST algorithm, using bands *i* and *j* is:

$$SST_{i,k} = a + b * T_i + c * T_k + f(d) \qquad (20)$$

where *i, k* take the numbers 20, 22 and 23, *f(d)* is a functional term than reduces the residual errors. In some circumstances these were found to be dominated by seasonal effects (Figure 10) and a suitable form of *f(d)* was found to be simply based on the solar declination:

$$f(d) = m * cos(2\pi(x + n)/365) + p \qquad (21)$$

where:

a, b ,c ,m ,n ,p are coefficients estimated separately for each of 3 latitudinal zones based distance from the equator.

d(northern hemisphere) = days after 173 (summer solstice)

d(southern hemisphere) = days after 357 (winter solstice)

T_{20} = BT measured in MODIS Band 20

T_{22} = BT measured in MODIS Band 22

T_{23} = BT measured in MODIS Band 23

for leap years, leap year days = standard year days *365/366

The values of the coefficients and residual SST errors are given in table 6, for atmospheres without aerosols, and table 7 for stratospheric aerosols present. For the clear atmosphere case the 22, 23 band pair is a very effective combination for compensating for the effects of atmospheric variability. The addition of more terms into the algorithm fails to reduce the already-low residual errors of the simple algorithm without explicit seasonal and regional terms. The use of band 20 introduces a larger dependency on the atmospheric variability, and for the 20, 22 and 20, 23 sets some improvement is gained by more complex formulations.

The presence of cold aerosols brings a significant dependency on the regional and seasonal variability (figure 10), which can be fairly well compensated for by the additional terms (table 7). As with the clear-air case the most effective band pair is 22 and 23.

The number of data points in the zone poleward is too few to make a stable estimate of the coefficients, so the global set are used (*pro tem*) in this zone. This contributes to the increase in ε(SST) seen in some cases when the data are partitioned into latitude zones, as does the presence of a few outliers that are excluded from the coefficient derivation, but are included in the estimation of the accuracy. It is expected that when the database is expanded with additional high latitude profiles that this anomaly will be resolved and the residual errors will decrease.

Residual uncertainties at nadir have rms values of 0.269K and 0.285K for bands 22:23 and 20:22 formulations.

Table 6. Coefficients and residual SST uncertainties (K) for the mid-range infrared bands, without stratospheric aerosols present.

Algorithm: Bands 22, 23	coefficients			ε(SST)
	a	b	c	
No seasonal	0.481199	1.62184	-0.613398	0.041
	m	n	p	
Seasonal	-0.010300	-33.856434	-0.003171	0.041
Seasonal+zonal:	m	n	p	
Lat: 23.45S - 23.45N	-0.014913	-44.695727	0.002888	
23.45 - 46.9 N or S	-0.010569	-9.100864	-0.012191	0.041
Poleward of 46.9 N or S	-0.010300	-33.856434	-0.003171	

Algorithm: Bands 20,22	coefficients			ε(SST)
	a	b	c	
No seasonal	1.63973	0.008332	1.01495	0.171
	m	n	p	
Seasonal	-0.02128	-27.77708	-0.010976	0.165
Seasonal+zonal:	m	n	p	
Lat: 23.45S - 23.45N	-0.021016	-65.4177	0.018011	
23.45 - 46.9 N or S	-0.02128	-27.77708	-0.010976	0.164
Poleward of 46.9 N or S	-0.02128	-27.77708	-0.010976	

Algorithm: Bands 20,23	coefficients			ε(SST)
	a	b	c	
No seasonal	1.63771	0.799358	0.249784	0.303
	m	n	p	
Seasonal	-0.089330	-14.636338	-0. 039860	0.304
Seasonal+zonal:	m	n	p	
Lat: 23.45S - 23.45N	-0.096743	-47.855918	0.033071	
23.45 - 46.9 N or S	-0.052036	0.006510	-0.138790	0.291
Poleward of 46.9 N or S	-0.089330	-14.636338	-0.039860	

Table 7. Coefficients and residual SST uncertainties (K) for the mid-range infrared bands, with stratospheric aerosols present.

Algorithm: Bands 22, 23	coefficients			ε(SST)
	a	b	c	
No seasonal	-4.42966	1.83049	-0.804068	0.311
	m	n	p	
Seasonal	-0.221255	-24.2229	-0.0845033	0.255
Seasonal+zonal:	m	n	p	
Lat: 23.45S - 23.45N	-0.155476	-28.3669	-0.0212811	
23.45 - 46.9 N or S	-0.268708	-28.7625	-0.115324	0.269
Poleward of 46.9 N or S	-0.221255	-24.2229	-0.0845033	

Algorithm: Bands 20,22	coefficients			ε(SST)
	a	b	c	
No seasonal	-2.45285	-0.293750	1.31549	0.319
	m	n	p	
Seasonal	-0.183720	-25.6533	-0.0793516	0.264
Seasonal+zonal:	m	n	p	
Lat: 23.45S - 23.45N	-0.112998	-26.5060	-0.0079824	
23.45 - 46.9 N or S	-0.213912	-31.8919	-0.140964	0.285
Poleward of 46.9 N or S	-0.183720	-25.6533	-0.0793516	

Algorithm: Bands 20,23	coefficients			ε(SST)
	a	b	c	
No seasonal	-7.71579	0.151332	0.890689	0.400
	m	n	p	
Seasonal	-0.239423	-28.1987	-0.0681934	0.340
Seasonal+zonal:	m	n	p	
Lat: 23.45S - 23.45N	-0.155810	-32.8452	0.0112498	
23.45 - 46.9 N or S	-0.237422	-26.0701	-0.220756	0.387
Poleward of 46.9 N or S	-0.239423	-28.1987	-0.0681934	

Analyses during algorithm development revealed that certain band differences are a good proxy for total column water vapor (figure 11). Plotting the regression residuals vs. radiosonde total vapor (*w*), the relationship is best for $-1K \leq (T_{20}\text{-}T_{22}) \leq 1K$ and $0 \leq w \leq 60$ kg m^{-2}. It is similar, but noisier (especially drier atmospheres), for $-0.5K \leq (T_{20}\text{-}T_{23}) \leq 2K$ and $0 \leq w \leq 60$ kg m^{-2}. The $T_{22}\text{-}T_{23}$ difference shows virtually no dependence on water vapor load, and is noisy for drier atmospheres. This indicates the water vapor is active in band 20. The main contamination in bands 22 and 23 is caused by the strong CO_2 absorption at 4.3 μm, which is not highly variable around the globe. This result is encouraging in that is provides a possible way of explicitly accounting for water vapor in the retrieval process without resorting to additional satellite data, such as the SSM/I on the DMSP satellites [*e.g.* Emery *at al.*, 1994].
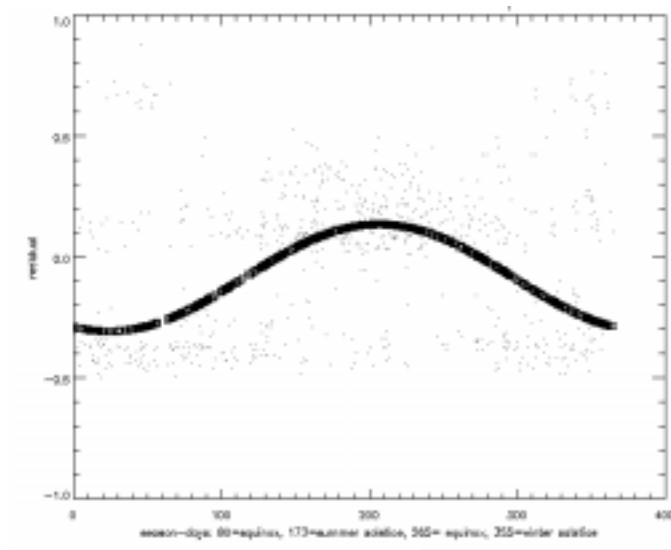
Figure 10. Seasonal correction function: modeled SST$_{22,23}$ versus day of year. Dots are simulated residual SST$_{22,23}$ errors prior to the addition of the seasonal correction to the algorithm; squares are the fitted seasonal correction function. The offset in the phase of the curve defined by the squares with respect to the dates of the solstices reflects the thermal inertia of the ocean-atmosphere system to the changing solar forcing.

Current research on this algorithm is focussed on the inclusion of zenith angle effects in the algorithm formulation; methods of including explicitly the information about atmospheric water vapor in the retrievals; and the use of the ECMWF pseudo-profiles to generate a set of coefficients based on a broader set of atmospheres.
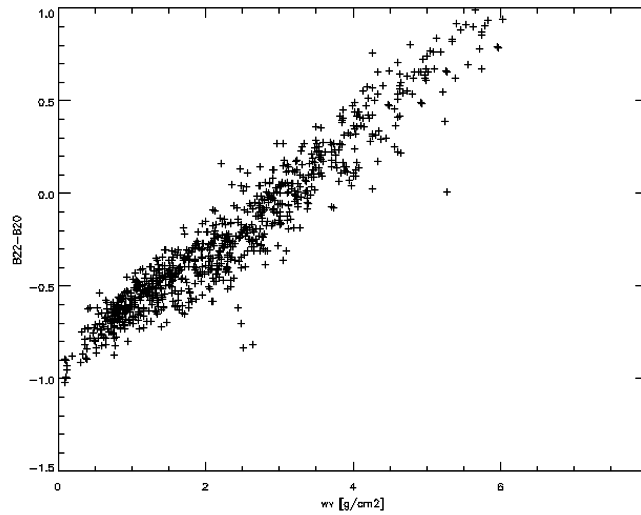
Figure 11 Simulated $T_{22} - T_{20}$ versus water vapor

3.2.4. Error budget

As stated above there are three processes that influence the MODIS infrared measurements: a) processes at the ocean surface that control the infrared emission; b) processes in the atmosphere that modify the infrared radiation between the surface and the aperture of the instrument; and c) the instrument characteristics. Uncertainties exist in all of these that are introduced by limitations on how well we understand the physical or instrumental processes or by natural variability in the environment that is imperfectly compensated in the measurement or in the data manipulation. These result in errors in the SST retrieval. The size of the errors can be estimated using a root-sum-square summation of the individual components, provided these are uncorrelated (see 3.1.3).

Considering the at-launch algorithm using measurements from bands 31 and 32, the residual uncertainties contributed by atmospheric variability are 0.337K at nadir and ~0.48K at a satellite zenith angle of 45°. The contribution from uncertainties in the surface emissivity results in typical SST errors of 0.05K [Watts *et al.*, 1996].

Recent information from the MCST show that both of these bands (31 and 32) have significant instrumental uncertainties (Table 8), and these propagate through the MODIS SST retrieval algorithm to produce amplified errors in the SST.

Table 8. Major component of error sources, specific to MODIS design, compared to those of AVHRR and ATSR

Source of uncertainty	MODIS (Bands 31 and 32; Ltyp)	AVHRR 11,12 μm channels	ATSR 11,12 μm channels
Scan mirror emissivity	>0.25K, occurs both in earth view and space view for in-flight calibration	N/A - constant angle of incidence	
Temperature of BB	<0.1K	?	<0.03K
Emissivity of BB	>0.995	?	>0.999
NEΔT	0.03 - 0.06K	0.05K (?)	0.02-0.04K

Ltyp – typical radiance measurement

BB – onboard black-body calibration target

When these are added (RSS) to the uncertainties introduced by atmospheric variability, we obtain a range of uncertainties in the derived SST that depend on the degree of correlation between the sources of instrumental error, and the atmospheric path length. These are given (1σ):

> Uncorrelated errors:
> > At nadir: ε(SST) = 1.09 to 1.42K.
> > At 45°, ε(SST) = 1.16 to 1.62K
> Correlated errors:
> > At nadir, ε(SST) = 0.45K
> > At 45°, ε(SST) = 0.56K

The spread of values in the uncorrelated errors indicates the spread caused by different types of atmospheric conditions. These estimates do not include electronic and optical cross-talk between the bands, residual cloud contamination and aerosol effects.

Although the MODIS pre-launch characterization is very extensive and has revealed much about the expected behavior of the instrument once in orbit, remaining uncertainties, especially in the scan-mirror reflectivity as a function of scan angle (rvs), contribute large components to the error budget.   No reliable system level measurements of the rvs in bands 20, 22, 23, 31 and 32 have been made and analysis by

the MCST of piece component measurements (including laboratory measurements of rvs on mirror witness samples) indicate residual uncertainties of greater than 0.1K under typical conditions. Because the angle of incidence of the radiation on the scan mirror changes across the swath, and is different for the measurements of the on-board black-body calibration target and for the cold space view used in the infrared band calibrations, the residual instrumental rvs uncertainties contribute to the error budget for each pixel through several routes. As a result the anticipated accuracies in SST are not likely to improve on those generally accepted to be characteristic of SSTs from AVHRR. To improve this situation it is planned to use in-orbit maneuvers which will rotate the spacecraft so the MODIS earth-view port is pointing to cold space to enable measurement of a uniform cold target across the MODIS scan. It is hoped that these will significantly reduce the residual rvs uncertainties. Table 9 gives the anticipated improvement in the SST retrieval uncertainties if these can be reduced to 50% and 10% of the current, pre-launch level. The achieve parity with the heritage instruments requires residual uncertainties at the ~10% of current level, and well correlated between the bands.

Table 9. Anticipated improvements in SST errors resulting from reductions in the MODIS rvs uncertainties.

	Uncorrelated		Correlated	
	Nadir	45° zenith angle	Nadir	45° zenith angle
If rvs uncertainties reduced to 50%	1.038K	1.256K	0.397K	0.526K
If rvs uncertainties reduced to 10%	0.641K	0.802K	0.359K	0.493K

4.2.5. Aerosol effects

Recent studies of the error characteristics of the AVHRR Pathfinder SST data set (see the ATBD of R.H. Evans) indicate that atmospheric aerosols are a major source of residual errors in situations that are classified as cloud free. These errors are often localized in areas of known aerosol outflows, such as Saharan dust off northwest Africa.

The published literature on the infrared properties of aerosols is very sparse, and such information that is available suggests there to be relatively little spectral structure in the aerosol infrared signatures. The aerosol parameters of d'Almeida, Koepke and Shettle [1991] have been used in an initial simulation study of aerosol effects on the
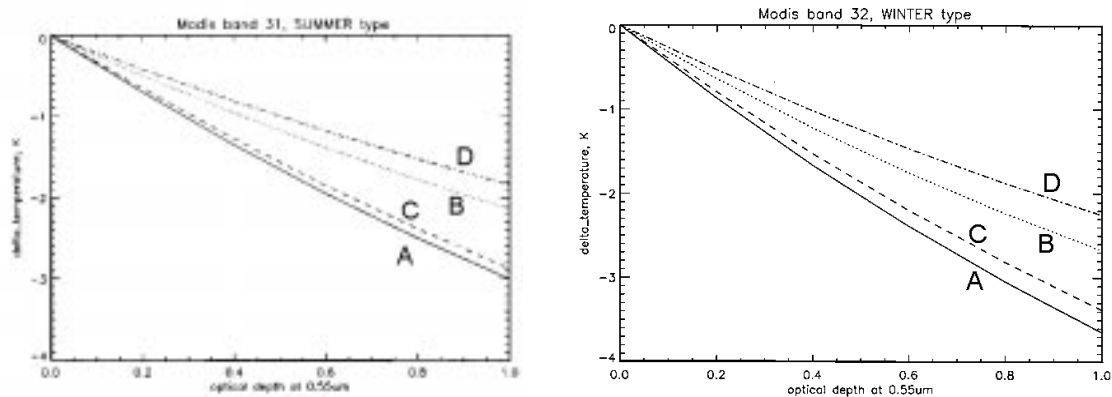
Figure 12. MODIS thermal infrared band bright ness temperature depressions that result from the effects of atmospheric aerosols. The left panel is for summer aerosol type, band 31; the right for winter aerosol type on band 32.

> A – tropical atmosphere – aerosols centered at 2km height
> B - tropical atmosphere – aerosols centered at 1.5km height
> C – temperate atmosphere – aerosols centered at 2km height
> D – temperate atmosphere – aerosols centered at 1.5km height

infrared MODIS bands using the RAL radiative transfer model. Two aerosol types were used – a winter and summer type. Aerosols were included in the model with a realistic size distribution spectrum and number density which allowed reference to the aerosol optical depth in the visible part of the spectrum (λ=550 nm). Two height profiles were used, each beginning at an altitude of 0.5km and extending to 2.5 km or 3.5 km, with a sin^2 envelope, *i.e.* centered at 1.5 and 2.5 km. Examples of the band brightness temperature depression for MODIS bands 31 and 32 are shown in Figure 12, for tropical and temperate atmospheres

The modeled aerosol effects produce very significant depressions in the brightness temperatures, and these show a nearly linear dependence on the aerosol visible optical depth. The dependences shown in Figure 12 are consistent for all of the simulations in that the most important variable is the height of the aerosol layer, while the consequences of different types of atmosphere is much less significant. The spectral behavior is very similar to that caused by water vapor ($T_{32} < T_{31}$) which means in practical applications the separation of aerosol and clear-air effects will be very difficult. To implement an aerosol correction scheme will require additional information, specifically the aerosol height distribution, and type, as well as the optical depth. Whether such information can be provided by MODIS to sufficient accuracy remains to be seen.

The spectral smoothness of these results is a direct consequence of the lack of significant spectral information in the available parameterizations. Recent results, however, of joint analysis of AVHRR and SeaWiFs measurements in situations of Saharan dust outflow over the sea off northwest Africa have revealed a spectral dependence that results, in some cases at least, of $T_{32} > T_{31}$. This signature is clearly different from that caused by water vapor and holds the potential of a mechanism for identifying aerosol contaminated MODIS data without resorting to external measurements. This is the subject of continuing research.

3.2.6. Polarization effects

The spectral emissivity of water exhibits polarization dependence, being somewhat higher for *p* polarization (vertical) than for *s* polarization [Friedman, 1969]. As a consequence, the brightness temperature (BT) measured for off-zenith emission is higher for *p* polarized radiation. As the radiation propagates through the atmosphere, the absorption and re-emission, and scattering, serves to reduce the polarization ratio, so the degree of polarization of the radiation at the top of the atmosphere is dependent on the state of the atmosphere as well as the surface emission angle. As a result of the reflections at various surfaces of the optical path of MODIS, the infrared bands are polarization sensitive, and consequently errors in the BT measurements may result. These would take the form of bias errors varying across the MODIS swath (emission angle effect), modulated by the atmospheric state.

The polarization effects were simulated in the RAL radiative transfer model for three types of atmosphere (tropical, mid-latitude and high latitude), for the extreme case of 1000 km across-track distance (very close to 60° emission angle). The results are shown for the MODIS bands in Table 10.

The ratios of the photon fluxes at the top of atmosphere, reduced by the polarization mixing effect of the atmosphere, are smaller than the ratio of surface emissivities. This effect is much more pronounced for the less transmissive tropical atmospheres at long infrared wavelengths. The emissivities are lower at the short wavelength bands, hence the ratio of the photon fluxes are down to about 0.9, but here the ratio is less effected by the amount of water vapor so variations caused by the atmosphere are much less. The consequent BT differences are appreciable, but these values are reduced by the

polarization sensitivity of the instrument in each band. Measurements from which the MODIS band polarization sensitivities can be derived were made during the pre-launch characterization, but at present are not available. However, a comparable study of the polarization sensitivity of the ATSR [Edwards *et al.*, 1990; Minnett, 1995a & 1995b], which has a much simpler optical path, produced errors (where error means the difference between BTs derived from the same photon flux, in one case polarized, in the other unpolarized) at an emission angle of 55° of 0.9mK, 1.5mK and 4.2mK, for the tropical, mid-latitude and high latitude atmospheres.

Table 10. The effects of polarization of the infrared emission at a distance of 1000km from the sub-satellite point for selected MODIS bands.

Band	Emissivity ratio	Ratio of photon fluxes			BT difference (K)		
		Tropical	Mid-lat.	High lat.	Tropical	Mid-lat.	High lat.
20	0.875	0.913	0.908	0.983	2.114	2.157	2.178
22	0.882	0.908	0.907	0.882	2.320	2.257	1.962
23	0.883	0.935	0.937	0.938	1.608	1.514	1.270
29	0.907	0.975	0.961	0.928	1.272	1.973	3.200
31	0.945	0.997	0.990	0.957	0.207	0.660	2.413
32	0.907	0.996	0.986	0.931	0.272	0.995	4.225

This analysis will be continued when the MODIS polarization properties are better known, and, if necessary, an algorithm for the correction will be developed. This would have the across-track distance, the brightness temperature to be corrected, and a brightness temperature difference - indicating the atmospheric absorption magnitude - as its parameters.

3.3   Practical Considerations

Major areas of concern have to do with efficient implementation of the atmospheric correction codes. Given that a minimum of 7 x 10^8 pixels with 9 radiances must be processed daily (Order 10^{10} estimates), the calculation must be highly optimized - this implies an average processing of 10^4 pixels $\cdot$ s^{-1} just to stay current. Current proto-algorithm development benchmarking suggests that much of the calculation must be table driven and close attention must be addressed to efficient, fast mass storage access for the algorithm to be effectively implemented.

Specific aspects of the implementation include calculation of the black body temperature and efficient mechanisms for estimating temperature from radiances. The black body formula to be used is

$$B_T(v) = 1.19106759 \; x \; 10^{-5} \; v^3 \left[e^{1.43879 v/T} - 1 \right]^{-1} \qquad (22)$$

where v is the wavenumber in cm^{-1}, T is the temperature in K, and B is resultant blackbody radiance. Since this product requires level-1a calibrated radiances as inputs to the calculation, there is no specific calibration procedure. Now, we assume that the output of each MODIS infrared band count is proportional to input radiance, *i.e.*,

$$C_i = S_i L_i + I_i \qquad (23)$$

with C_i the count, L_i the incident radiance, and S_i, I_i the slope and intercepts for the ith band (Lauritson *et al.,* 1979, Brown *et al.,* 1985 provide analogous descriptions for NOAA AVHRR radiance computation).

Effective arithmetic implementation of the calibration step necessitates development of a counts-to-temperature look-up table which is computed one time and then offset, depending on changes in instrument internal operating temperature. Functionally one performs the following calculation:

$$T_B = \text{table (i)} \qquad (24)$$

where T_B is the respective brightness temperature for the band in question and table is the counts to brightness temperature look-up table.

3.3.1 Algorithm Builds

This document describes the pre-launch algorithm. There will be additional versions of the Sea_sfc Algorithm. The overall structure of the algorithm should remain reasonably stable, i.e., we expect the correction equation to be based on a combination of MODIS infrared bands. Our execution phase plan identifies a number of releases prior and post-launch.

3.3.2 Reprocessing

Provided there is no 'catastrophic' change to the atmosphere, such as a large volcanic eruption that injects large amounts of aerosols into the stratosphere, MODIS atmospheric correction algorithms will not change very quickly, however, our execution phase plan suggests that annual updates should be expected. All MODIS Sea_sfc Temperature Algorithm products should be identified with a version identification so that users can readily discern the algorithm used. We would propose that major reprocessing of MODIS infrared data be no more frequent than annual. Catastrophic atmospheric events will be dealt with, if they occur, in the best fashion possible.

3.3.3 Programming/Procedural Considerations

The computer code for the derivation of the skin SST using measurements from bands 31 and 32 (see section 3.2 above), has been delivered and has been tested at RSMAS. There is no concern about the processing burden on the computing facilities. Further details are given in the ATBD of MODIS Instrument Team member Dr. Robert Evans.

4.0 Calibration and Algorithm Validation

Calibration/Validation has two important aspects: prelaunch determination of instrument calibration and characterization in a thermal-vacuum test setting and validation of on-orbit performance. We assume that our role in the pre-launch efforts is an advisory role, *i.e.*, the MCST calibration and characterization activity will directly supervise the thermal-vacuum activities and deliver models to transform MODIS sensor counts into calibrated radiances which are valid over the on-orbit operating envelope.

On-orbit performance characterization consists of two aspects: assessing calibration model performance and assessing MODIS Sea_sfc Temperature algorithm performance. We assume that radiance calculated from instrument counts will be accomplished using calibration models provided by the MCST Calibration activity. We rely on the conversion to radiances being a reversible transformation from counts, i.e., no information is lost in going to and from counts to radiances. Please note, however, that raw count data may be required for selected sites in the calibration-validation effort. We will require continued access to the MCST calibration performance results in order to characterize the impact of the on-orbit calibration model performance on the algorithm performance. We will require access to the results, and possibly the raw data, form the planned space-view maneuver to characterize the scan mirror response *vs* scan angle (rvs). Depending on the results of the maneuver, it may be necessary to account explicitly for the rvs in the SST retrieval algorithm, or use these results in analyzing the validation data.

4.1   Post-launch Algorithm Through Validation

The infrared channels of MODIS form a self-calibrating radiometer. By using measurements of cold space and of an on-board black-body calibration target, the infrared measurements from the earth-scan are calibrated producing radiances in the spectral intervals defined by the system response functions of each channel. These calibrated radiances can be converted to brightness temperatures (i.e., the temperature of a black-body that would give the same channel radiance) at the height of the satellite. To derive an oceanic surface temperature from the calibrated radiances at satellite height (or top-of-atmosphere brightness temperatures) it is necessary to correct for the

effects of the intervening atmosphere. This is the role of the sea-surface temperature retrieval algorithm, sometimes referred to as the atmospheric correction algorithm.

The post-launch validation activities are designed primarily to test the efficacy of the sea-surface temperature retrieval algorithm, not primarily to validate the pre-launch characterization or in the in-flight calibration procedure. It is presumed that the pre-launch tests, supplemented by in-flight maneuvers, will provide adequate characterization of the instrument to engender confidence in the calibrated band radiance measurements. With this confidence, the validation measurements can be interpreted in terms of the performance of the atmospheric correction algorithm; without this confidence the separation between instrument performance and algorithm performance cannot be made and the interpretation of the validation data sets will be very difficult. Of particular importance in the pre-launch characterization are the determination of the spectral response functions of the MODIS channels, the quantification of "cross-talk" between channels, and the accurate description of the properties of the scan mirror as they change with scan angle. Failure to correctly characterize these before launch will seriously compromise our ability to understand the properties, strengths as well as weaknesses, of the SST retrieval algorithm and to demonstrate the validity of the derived SST fields.

4.1.1 Scientific Objectives

Several fundamentally different, but complementary, data sets are needed to provide an adequate sampling of the marine atmospheric conditions and sea-surface temperature (SST) that is necessary to validate the MODIS infrared band measurements and derived SST fields. Our validation strategy is two-fold: Highly-focused field expeditions using state-of-the-art calibrated spectral radiometers, supported by extensive instrument suites to determine the state of the atmosphere, are necessary to understand the atmospheric and oceanic processes that limit the accuracy of the derived SST. In addition, long-time period, global-scale data sets are necessary to provide a monitoring capability that would reveal calibration drift and the consequences of sudden or extreme atmospheric events, such as volcanic eruptions, transoceanic transport of terrestrial aerosols, cold-air outbreaks, etc. on the global SST product.

4.1.2 Missions

MODIS, and derivative instruments, are expected to be operational for about 15 years beginning with the launch of the AM-1 platform in 1999. It is our intent to use field programs that take place during the pre-launch and operational period as the basis of MODIS validation exercises. In particular, the DOE ARM (Atmospheric Radiation Measurements) program sites in the Tropical Western Pacific Ocean (TWP) and North Slope of Alaska and Adjacent Arctic Ocean (NSA-AAO) provide a valuable framework for MODIS validation as they provide an unparalleled selection of instruments to determine the state of the atmosphere [Stokes and Schwartz, 1994; Mather *et al.* 1998][2]. These sites will operate for about a decade, beginning in late 1996 for the TWP, and about 1997 for the NSA-AAO, at the extreme ranges of atmospheric and oceanic conditions. In addition to these two long-term sites, use will be made of the supplementary, oceanic ARM sites that are intended to be operated on a short-term basis, intermittently or for specific research campaigns. These include the eastern North Pacific or Atlantic Oceans (probably the Azores), the Gulf Stream off the eastern USA, and the Bering or Greenland Seas.

Opportunities to use other oceanic and marine atmospheric campaigns based on ships, buoys, fixed platforms, aircraft, and island stations will be grasped as funding and resources allow.

Pre-launch campaigns are being used to test strategies, constraints, and to develop the instrumental and computational tools that will be used in the post-launch validation, again as opportunities and funding allow. Examples of these include the Combined Sensor Program cruise to the Tropical Western Pacific in March-April 1996, the International North Water Polynya expedition in March-July 1998; and the Nauru99 Campaign in the Tropical Western Pacific Ocean in June 1999.

A map showing the tracks of ships used in the pre-launch studies is given in Figure 13, which includes some post-launch validation campaigns and others that are still under negotiation.

---

[2]   The ARM Sites, currently operational and situated in the Southern Great Plains centered near Lamont, OK, and at the North Slope of Alaska, at Barrow, AK, provide a valuable source of measurements for validation of land surface temperature: this parameter is not dealt with here.

MAERI Cruises
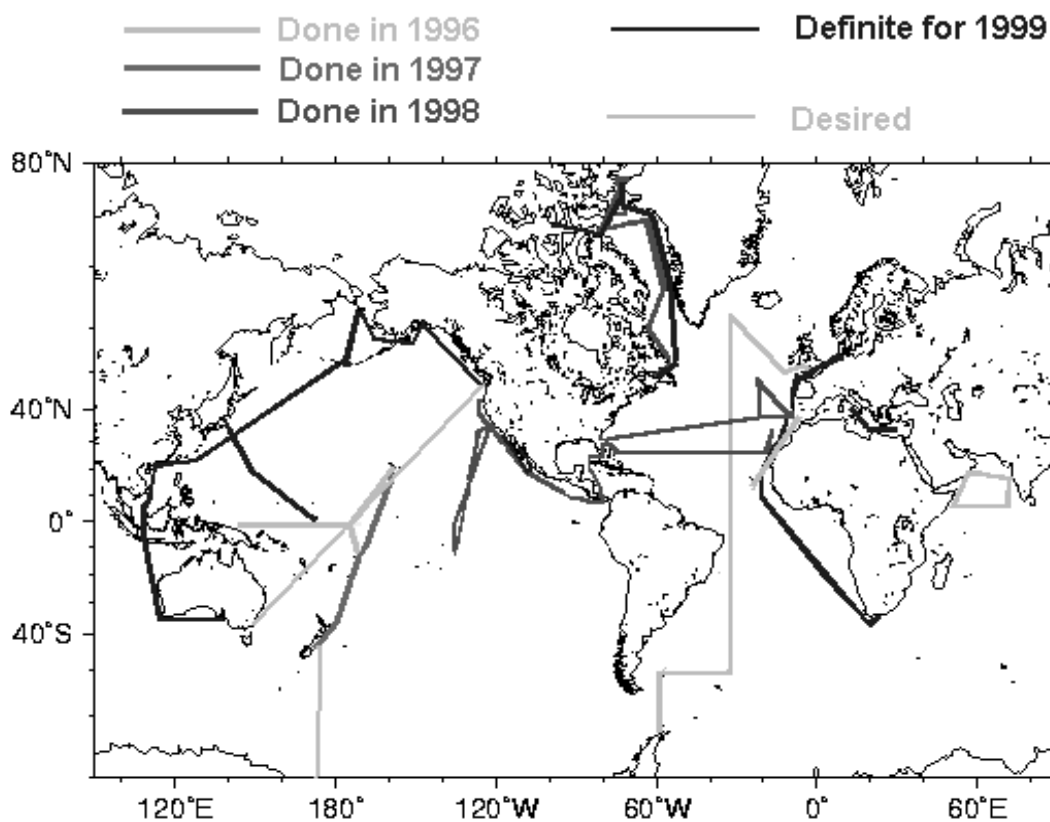
Figure 13. Schematic representation of the M-AERI cruises. Because of the Terra launch slip, two cruises in the Western Pacific (Australia to Seattle, via Hong Kong and Alaska; and Japan to the Equator and back) fall now in the pre-launch period. If the launch does indeed take place in late July 1999, the four remaining cruises in 1999 will constitute the initial validation dataset.

4.1.3 Science data products

The primary science data product to be validated is sea-surface temperature (MODIS Product number 28 / EOSDIS Product number 2527). To achieve this requires thorough characterization of the atmospheric and ocean surface variables that influence the SST retrieval from the MODIS band radiance measurements. The cloud mask to be provided by the MODIS Atmospheres Group (Paul Menzel) (EOSDIS Product number 3660) will be used to eliminate cloud contamination, but the influence of clear-air constituents, including aerosols, remains to be corrected. At the sea surface, the spectral emissivity together with its surface roughness and emission angle dependences must be taken into account. The sea-surface temperature retrieval is of course limited to the ice-free oceans: the ice-mask product (MODIS MOD29) will be used to delineate the ice-free areas.

4.2   Validation Criteria

Post-launch validation of the MODIS infrared bands is required to monitor the performance of the in-flight calibration procedure to detect possible degradation, to uncover potential instrument problems (such as possibly inadequate characterization of the angular dependent reflectivity of the scan mirror), but primarily to determine the effectiveness of the atmospheric correction algorithm. Ideally the accuracy and noise characteristics of the data being used in the validations should be superior to those of the MODIS measurements. This may be difficult to achieve, given the expected performance of MODIS.

4.2.1 Validation Approach

Validation is required over the lifetimes of the MODIS missions, and, the validating instruments must be deployed in situations that encompass the entire range of surface temperatures and atmospheric variability. Since no single approach provides a perfect validation measurement, a selection of techniques and instruments is required to provide an adequate validation data set. The approach includes (i) validation of top-of-the-atmosphere radiances, (ii) validation of surface radiances and (iii) validation of surface temperatures.

There are three possible methods of validating the top-of-atmosphere radiances:
- comparison with other satellite measurements
- comparison with aircraft radiometers underflying the satellite,
- using radiative transfer modeling to simulate the MODIS measurements.

Validation of surface radiances is achieved using calibrated spectroradiometers, such as the Marine-Atmospheric Emitted Radiance Interferometer [Smith *et al.*, 1996], or broad-band infrared thermometers. These instruments can be mounted on low-flying aircraft [Saunders and Minnett, 1990; Rudman *et al.*, 1994; Smith *et al.*, 1994], ships [Schluessel *et al.*, 1987; Smith *et al.*, 1996], or fixed platforms. Using in situ measurements employ those taken using conventional thermometers on free-drifting or moored buoys [Strong and McClain, 1984; Podestá *et al.*, 1997; see also the ATBD of Dr. R.H. Evans], and ships [*e.g.* Llewellyn-Jones *et al.*, 1984].

Wherever possible, synergism will be sought by collaboration with the validation efforts of the MODIS Ocean Color and MODIS Atmospheres groups, to leverage equipment and data. An example of this is the joint ocean color and SST campaign in the Eastern Pacific in October 1999.

4.2.2 Sampling requirements and trade-offs

Comparison with other satellite infrared radiometers has the advantage of comparing similar measurements. The problems in such an approach are in the possible changes in the top-of-the atmosphere radiation field between the two satellite overpasses (resulting from changes in the surface temperature and/or in the intervening atmosphere), differences in the viewing geometry of the two satellites, differences in the spectral responses of the different satellite instrument bands, and possibly inadequate accuracy or noise characteristics of the validating instrument. Another possible problem is the potential for undetected in-flight degradation of the validating radiometer - if systematic discrepancies are found it may not be apparent which satellite sensor is at fault.

A significant advantage of using aircraft radiometers is that the data can be taken simultaneously with the MODIS measurements. However, because of the difference in spacecraft and aircraft speeds, truly coincident measurements will be very few, but within, say a 30-minute window of the satellite overpass a large number of validation measurements could be obtained, (precise interval to be determined; Minnett, [1990]). Also, the aircraft radiometers can be arranged (in principle) to match the MODIS viewing geometry, and can be scheduled (again, in principle) to avoid conditions that would make data interpretation difficult (*e.g.*, broken cloud fields). Disadvantages of this technique include the effects of the atmosphere above the aircraft, which can be accounted for by modeling using an assumed (or measured) temperature and humidity profile, and the accuracy of the aircraft instruments. Candidate aircraft instruments for top-of-the atmosphere radiance validation of the bands used in SST determination include the MAS (MODIS Airborne Simulator; King and Herring, [1992]) and the HIS (High-Resolution Interferometer Sounder; [Bradshaw and Fuelberg, 1993]). These instruments are flown typically on the NASA ER-2 research aircraft at a height of ~20km, and under these conditions the spatial resolution is 50m (MAS) and 2km (HIS). The noise levels of the instruments are not as low as those for the MODIS infrared bands (see table in 4.3). For the MAS the NEΔT is ~0.3K for a target at ~290K for the 3.7-4.0µm bands and 0.1 - 0.2K for the 11-12µm bands, but these could be greatly improved

(by a factor of 20 if the noise were truly random) by averaging the data down to the MODIS spatial resolution of ~1km^2. The noise levels in the HIS spectra in the 800 to 1050 cm^{-1} interval are typically 0.2-0.45 mW m^{-2} st^{-1} cm, and these result in an uncertainty in the skin SST retrieved from the HIS spectra of ~0.15K [Nalli, 1995; Nalli and Smith, 1998].

The use of numerical models of the radiative transfer through the atmosphere to simulate the satellite measurements requires high quality measurements of the relevant atmospheric properties (temperature and humidity profiles, aerosol characteristics) and emitted radiance at the surface taken at the time of the satellite overpass. Advantages of this approach are that a large data-base of measurements can be generated over an extended period of time and representing a large range of atmospheric conditions, surface temperatures, and viewing geometries for relatively modest outlay. Disadvantages are the uncertain accuracies of the atmospheric profiles, generally derived from routine radiosonde measurements [Schmidlin, 1988], and shortcomings in the parameterization of incompletely understood physical processes in the radiative transfer model, such as the atmospheric water vapor anomalous continuum absorption and emission, and the effects of tropospheric and stratospheric aerosols.

The long-term measurement of surface emitted radiance, or the band brightness temperatures, at the surface serves to monitor the behavior of the atmospheric correction algorithms as well as the MODIS performance. The surface measurement is of emitted radiance plus the reflected component of the downwelling radiance originating in the atmosphere. The MODIS space based measurement is of this combination, after attenuation by atmospheric absorption and scattering, plus the radiance emitted or scattered by the atmosphere into the MODIS field of view. This validation measurement is therefore less direct than a top-of-atmosphere comparison. Surface measurements can be related to the MODIS measurement by using a radiative transfer model to provide an estimate of the atmospheric attenuation and upwelling and scattered radiation, or by converting the surface measurement to a temperature and comparing it with the surface temperature derived from the MODIS measurements. In either case, the successful interpretation requires a good description of the atmospheric and surface properties (skin SST, surface emissivity and wind speed). In the latter case a measure of the downwelling radiation is required to derive the temperature from the surface measurements. This can be achieved by pointing the surface radiometer at the sky. Suitable instruments include the AERI (Atmospheric Emitted Radiation

Interferometer) or, for use at sea, the Marine-AERI (M-AERI), and broad-band infrared thermometers [Smith *et al.*, 1996]. The M-AERIs have internal black-body calibration targets and so provide a calibrated measurement. They measure the spectrum of infrared radiation in the range from 3.3 to 18 μm with a spectral resolution of ~0.5 cm^{-1} These spectra can be compared to the MODIS measurements by multiplying them by the MODIS normalized band spectral response functions. The M-AERI spectra can also be analyzed to derive surface temperature and emissivity, and, using spectra of sky radiation, the temperature and humidity structure of the atmosphere.

Broad-band infrared radiation thermometers have the advantage over M-AERIs in that they are inexpensive. They usually do not have the required accuracy of 0(0.1K) and have a simple internal calibration procedure (if any). However, recent experience with some types indicates they may produce useful observations, and may be suitable for deployment in larger numbers on platforms of opportunity.

Surface temperature thermometers can be deployed in plentiful numbers to provide adequate monitoring of MODIS performance in principle. However, they have a big disadvantage in that their measurement may be decoupled from the MODIS measurement by near-surface temperature gradients. For sea surface temperature the in situ thermometer is immersed in the water, frequently at depths of 0(1m) and its measurement may differ from the temperature of the radiating skin of the ocean by >1K. These gradients are caused by heat exchange between ocean and atmosphere [the skin effect; *e.g.* Robinson *et al.*, 1984; Schluessel *et al.*, 1990] or by diurnal heating in conditions of low wind speed and therefore reduced surface mixing [*e.g.* Stramma *et al.*, 1986]. Despite this problem in situ thermometers have been used extensively to validate satellite SST's [*e.g.* Strong and McClain, 1984; Llewellyn-Jones *et al.*, 1984; Podestá *et al.*, 1997].

4.2.3 Measures of success

The results of the validations will be used to revise the atmospheric correction algorithms used in the SST derivation. The algorithms will be refined until the accuracy goals of the MODIS mission have be reached, in as much as this can be demonstrated within the constraints imposed by the methods of determining the absolute accuracy of the MODIS SST measurement.

4.3 Pre-launch algorithm and test/development activities

An extremely important aspect of the pre-launch activities is the full characterization of the infrared bands of the MODIS flight models. This includes giving a complete of definition of the spectral and spatial responses of the individual bands; specifying the properties of the elements used in the in-flight calibration procedure, and providing a good description of the thermal conditions expected in and around the instrument in orbit. Without this information, the interpretation of the data derived from the validation exercises will be very difficult.

Pre-launch validation activities have been directed towards validating the atmospheric correction algorithm formulation using AVHRR data, refining validation instruments and determining the best strategies for the post-launch validation.

The primary instrument for the surface validation of the MODIS infrared bands is the Marine-Atmosphere Emitted Radiance Interferometer (M-AERI), and part of the pre-launch activities has been directed to ensuring the accuracy of the instrument, testing it under sea-going conditions, and developing the necessary software.

4.3.1 M-AERI

The M-AERI is a development of the AERI (Atmosphere Emitted Radiance Interferometer), an instrument developed at the Space Science and Engineering Center at the University of Wisconsin-Madison for the Department of Energy Atmospheric Radiation Measurement Program [Stokes and Schwartz, 1994; Mather *et al.*, 1998], and of the airborne High-Resolution Interferometric Spectroradiometer (HIS) which has been flown on the NASA ER-2 research aircraft [Revercomb *et al.* 1988]. A prototype instrument was tested at sea in a proof-of-concept experiment in the Gulf of Mexico in January 1995, where it performed very well. It demonstrated an ability to measure skin temperatures that agreed well with near-surface in situ measurements, and deviated in the manner expected from consideration of surface heat exchanges [Smith *et al.*, 1996]. Building on the experiences of this cruise, a more rugged M-AERI was developed, was used during the Combined Sensor Program (CSP) cruise in the Tropical Western Pacific in spring 1996 [Post *et al.*, 1997]. In addition to testing the instrument in extreme conditions, this cruise furnished an extremely valuable data set to study the effects of the tropical atmosphere on infrared satellite SST measurements including the spatial and temporal correlation characteristics of the relevant atmospheric constituent, the

near-surface horizontal and vertical thermal gradients. There are now three sea-going models of the M-AERI, which will be used for MODIS skin SST validation.

4.3.1.1 The instrument

The M-AERI (figures 14 and 15) is a Fourier-Transform Interferometric Radiometer which operates in the range of infrared wavelengths from ~3 to ~18μm (~500 to ~3000 cm^{-1}) and measures spectra with a resolution of ~0.5 cm^{-1} (Figure 16). It uses a sandwich of two infrared detectors (Indium Antimonide and Mercury Cadmium Telluride) to achieve the wide spectral range, and these are cooled to ~78°K by a Stirling cycle mechanical cooler to reduce the noise equivalent temperature difference to levels well below 0.1K. The M-AERI includes two internal black-body targets for accurate real-time calibration. A scan mirror directs the field of view from the interferometer to either of the black-body calibration targets or to the environment from nadir to zenith. The mirror is programmed to step through a pre-selected range of angles. When the mirror is angled below the horizon the instrument measures the spectra of radiation emitted by the sea-surface, and when it is directed above the horizon it measures the radiation emitted by the atmosphere. The sea-surface measurement also includes a small component of reflected sky radiance. The interferometer integrates measurements over 45 to 90 seconds per view (dependent on the NEΔTs of the detectors - M-AERI 02 has lower noise detectors than M-AERI 01 and therefore requires less time per spectrum) to obtain a satisfactory signal to noise ratio. A typical cycle of measurements including two view angles to the atmosphere, one to the ocean, and calibration measurements, can take less than 4 minutes. The M-AERI is equipped with pitch and roll sensors so that the influence of the ship's motion on the measurements can be determined, and with a GPS receiver so that accurate time and location are recorded for each measurement.
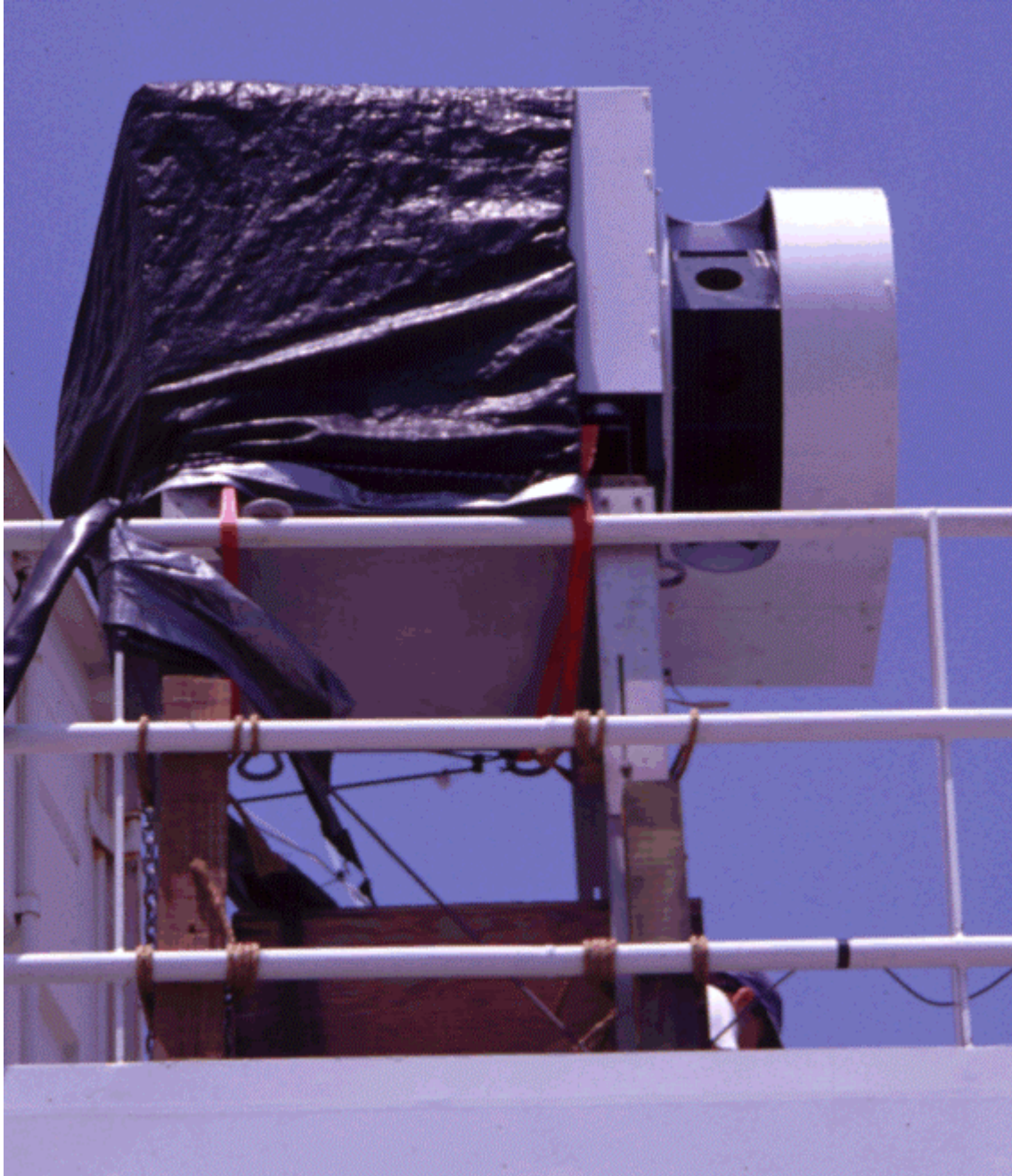
Figure 14. The M-AERI mounted on the NOAA S *Ronald H Brown*. The photograph was taken from the quayside, roughly in the field of view of the instrument.

Figure 15. The Marine-Atmosphere Emitted Radiance Interferometer (M-AERI). The inside of the instrument is shown above, with the Interferometer in the dark gray box with dark panels. The optical bench is double shock-mounted to damp vibrations. The light-gray assembly above contains some of the optical elements and the Stirling Cycle cooler is attached to the left. The detectors are below the silvered unit at the top. The front end is shown at left, with the two black-body calibration targets in the metal tubes. The dark cylinder in the hexagon contains the stepper motor for the gold scene mirror.
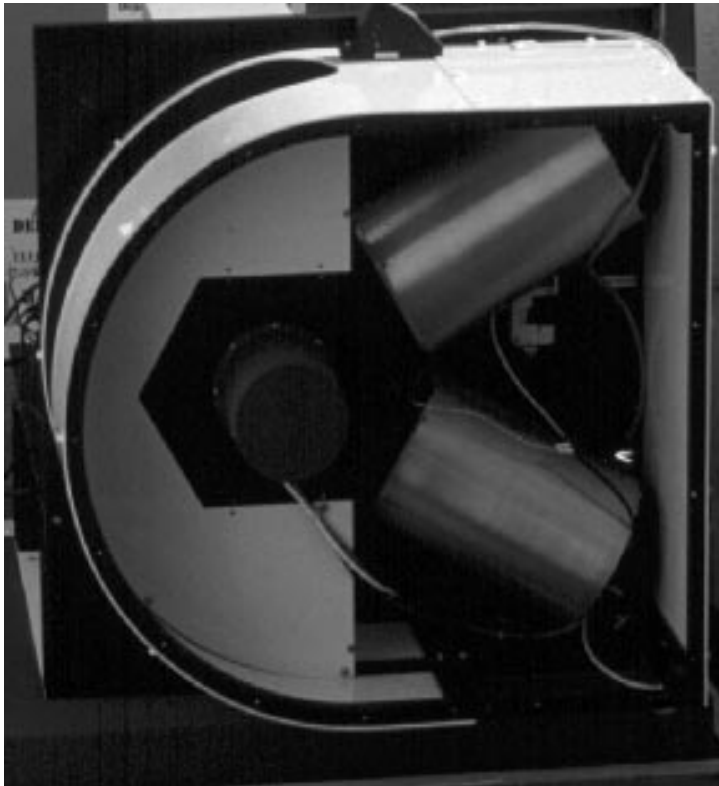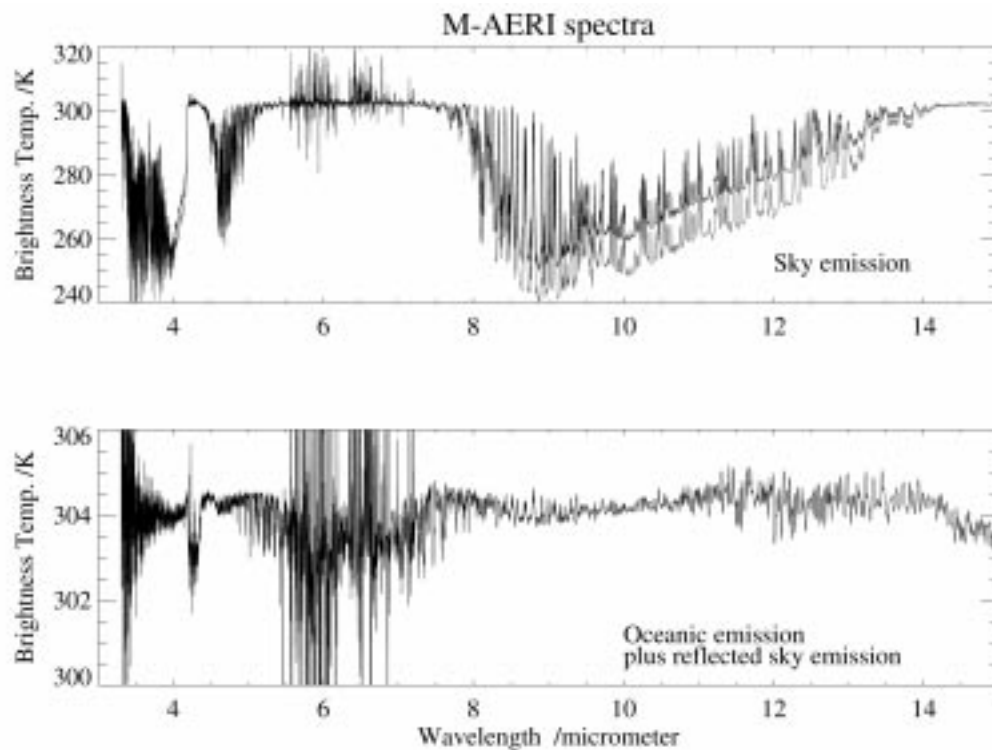
Figure 16. Spectra of emitted sky radiation (top) and upwelling radiation measured by the M-AERI taken in the tropical Western Pacific Ocean on March 24, 1996. Atmospheric measurements are at 45° and zenith (red), above; ocean measurements at 45° below the horizon, below. The cold temperatures in the sky spectra are where the atmosphere is relatively transparent. The 'noise' in the 5.5 to 7 μm range is caused by the atmosphere being so opaque that the radiometer does not "see" clearly the internal black body targets. The spectrum of upwelling radiation (lower panel) consists of emission from the sea surface, reflected sky emission and, in the spectral regions where the atmosphere is very absorbing, emission from the atmospheric path length between the sea surface and the radiometer. Analysis of the spectra of the upwelling radiation and the sky radiance yields both the sea–surface skin temperature and spectrum of the sea–surface emissivity.

4.3.1.2 Operations

The M-AERIs are designed to run continuously under computer control. At midnight UTC the computer reboots and ensures there is enough disk space for the new day's measurements. If the available disk space is too small, the oldest day's data are deleted, so to avoid data loss operator must write the previous day's measurements to CD or tape. While causing a small (few minutes) loss of data, the daily reboot serves to identify and rectify any residual problems that may have resulted from anomalous situations in the instrument, computer or software that may not be apparent to the operator and which may eventually lead to a system crash.

To assist the operator monitor the status of the instrument and data flow, the M-AERI is equipped with a range of sensors that report on the state of the hardware. Also, the data acquisition software applies real-time quality-assurance checks to both the interferometer data stream and these 'housekeeping' measurements. Several of the parameters are plotted in real-time as time-series on the screen of the control computer. Anomalous behavior is usually identified quickly by the alert operator. Also, the values of 48 critical variables are checked against pre-set threshold values, and when these are exceeded, a visual warning is issued in the form of small panels on the display screen changing color from green to yellow to red. Finally, the computer issues audible and visual warnings when there is a loss of communication between the computer and the FTIR itself. This is caused either by a problem with the cable or connectors, or by the internal temperature of the FTIR falling or rising outside of the operating range. To summarize, much attention has been paid to ensuring a minimum of data loss during the routine operation of the M-AERI.

One source of data loss, however, is contamination of the scan mirror by heavy rain or sea spray. The mirror must remain clean and dry for the M-AERI to provide the required measurements. A Vaisala rain sensor is mounted close to the M-AERI aperture and when the output from this crosses a pre-determined threshold, the mirror is moved into a 'safe' position. The mirror is enclosed in a metal cylinder with a circular aperture in the side, for the field of view, which rotates with the mirror. In the 'safe mode' the mirror surface is directed to the lower, ambient-temperature, black-body calibration cavity, and the back of the mirror cylinder is presented to the rain or spray. When the rain sensor output recovers through the threshold value again, the mirror scan sequence is resumed. There is the option of an operator over-ride of the automatic mirror 'safing' mechanism that causes the mirror to immediately enter or exit the safe mode. When the risk of salt spray entering the instruments is high, and during heavy rain, the M–AERI is covered for protection and no useful data are collected. Similarly, when there was evidence of direct sunlight entering the aperture, a shield is used which obscures some of the environmental views at the affected mirror angles.

The sea surface interfacial temperatures are retrieved from the 55° sea and sky view data using measurements in a narrow spectral interval at 7.7µm (1302.0 to 1307.0 cm^{-1}), where the atmosphere is only moderately transparent [Smith *et al.*, 1996]. The emissivity used in the retrievals is 0.962627 [Wu and Smith, 1997]. This is somewhat smaller than the value in the 10-12µm interval where SST is conventionally measured

by infrared radiometry. However, at the longer wavelength interval, where the atmosphere is relatively transparent, the reflected component has its origin higher in the atmosphere, and so is much colder that the radiation originating at the interface. It is also sensitive to the presence of low clouds, which insert a warm radiation source in the reflected sky radiation. Thus, even if the reflected component is larger at 7.7µm than at 10-12 µm, the correction for sky radiation is less dependent on the cloud conditions, as nearly all of the reflected sky radiation has its origin in the lower troposphere. Uncertainties in the correction for the reflected component are dependent on the temperature difference between the surface and the source of the atmospheric component, which is much smaller at 7.7µm than 10-12 µm

The tilting of facets of the sea surface by the wind [Cox and Munk, 1954] induces an apparent wind-speed dependency of the emissivity and therefore also the reflectivity. Recent modeling results [Watts *et al.*, 1996; Wu and Smith, 1997] show that the wind-speed dependence to be much smaller than indicated in earlier studies [Masuda *et al.*, 1988], and to be small for emission angles less than 60°. Thus the interfacial temperatures derived from measurements at 55° of emission at 7.7µm are relatively free of contaminating effects.

4.3.1.3 Accuracy

Great attention is paid at SSEC during the construction of the M-AERIs to ensure that the measurements are as accurate as possible. The design goals are absolute uncertainties in the derived SST of <<0.1K, which is a very demanding target. The absolute accuracy rests with the accuracy of the M-AERI internal black-body calibration cavities, one of which is heated to 60°C and the other 'floats' at ambient temperature. These are designed as cylindrical cavities with a concave conical base. Ray tracing simulations indicate that 81% of the emergent radiation comes from this apex and the remainder from the side-walls of the cavity. The temperature of each cavity is monitored by three thermistors, which have been specially calibrated with traceability to NIST standards. Because the SST is very close to ambient air temperature the uncertainties in the SST are most influenced by those in the ambient temperature black-body cavity, but since this is not activity heated or cooled the internal temperature gradients are minimal and confidence in its temperature measurement is high.

The cruise of the R/V *Roger Revelle* from Hawaii to New Zealand in autumn 1997 (see Table 14 below) presented the opportunity to use two M–AERIs (Models 01 and 02) with to compare co-located skin temperature measurements from two independently calibrated instruments. Both M–AERIs were mounted side-by-side on the forward 02 deck viewing undisturbed ware ahead of the ship's bow wave. The fields of view at the sea surface were not superimposed and the measurements were not synchronized. A point-by point comparison is not possible, but a statistical analysis of the two time series, with the measurements of M-AERI 01 interpolated to the times of those of M-AERI 02 produced excellent results (Table 11).

Table 11 . M-AERI Skin SST comparisons. R/V *Roger Revelle* cruise, Hawaii to New Zealand, October 1997.

Date - UTC	N	Mean Δ_mT /K	St.dev. Δ_mT /K
October 1	70	0.005	0.033
October 2	58	0.020	0.084
October 3	56	0.002	0.092
October 4	85	0.005	0.059
October 5	56	0.000	0.091
October 6	79	0.021	0.067
October 7	146	0.000	0.073
October 8	74	-0.003	0.085
October 9	133	0.009	0.062
October 10	133	-0.003	0.099
October 1-10	**890**	**0.005**	**0.077**

- *SST derived at 55° incidence angle, λ = 7.7 μm*
- *Δ_mT = Skin SST (M-AERI 02 –– M-AERI 01)*
- *M-AERI 01 data interpolated to times of M-AERI 02 measurements*
- *N is the number of independently calibrated data point in each 24 h data segment*

These results show that the M-AERI is capable of measuring skin temperatures with an accuracy of a few mK for daily averages, with uncertainties of <<0.1K for individual measurements (remembering that some of this variability is the result of lack of collocation and simultaneity in the two data sets). However, since both M-AERIs were built in the same laboratory there is the risk that a bias error has crept into the calibrations through the use of a common facility.   An infrared radiometry workshop held at UM-RSMAS in March 1998 [Kannenberg, 1998] provided the means of testing the absolute calibration of the M-AERIs, and other radiometers, used at sea against a

range of calibration targets. One of these was provided by NIST, which used a water bath to provide temperature stability to the black cone target, and this was used to check the absolute radiometric accuracy of a M-AERI (model 02). Measurements were taken with the NIST calibration target at 20ºC, 30ºC and 60ºC. The results are summarized in table 12 and figure 17[3].

Table 12. Mean discrepancy in the M-AEI 02 measurements of the NIST water bath black-body calibration target in two spectral intervals. Miami IR Workshop 2-4 March 1998.

Test Temperature	LW (980-985 cm^{-1})	SW (2510-2515 cm^{-1})
20ºC	+0.013 K	+0.010 K
30ºC	-0.024 K	-0.030 K
60ºC	-0.122 K	-0.086 K

Discrepancies are M-AERI minus NIST

The results of the M-AERI 02 – NIST comparison show very small absolute uncertainties, especially at 20 ºC, i.e. close to ambient temperature. The increasing discrepancies with increasing temperature can be explained if the effective emissivity of the NIST target is about 0.998. When used on ships, the M-AERI SST measurement is of a temperature close to ambient, and is taken at the wavenumber interval of 1302.0 to 1307.0 cm^{-1} where the absolute calibration uncertainties are very small indeed.

As a result of these measurements taken in the laboratory and in the field, we have confidence in the absolute accuracy of the skin SST measurements being well below the design objective of <0.1K.

4.3.2. Ancillary measurements

To provide measurements of the environmental conditions in which the M-AERI measurements are made, a suite of ancillary sensors are usually also deployed on the ships (Figure 18). Measurements of the surface layer meteorological variables are usually made during many of the M-AERI cruises using a Coastal Environmental Systems Weatherpak System (Table 13). Because the skin temperature of the ocean is responsive to cloud cover, an all-sky camera is used to record the cloud conditions.

---

[3] Table and figure kindly provided by Dr. R.O. Kunteson, SSEC, University of Wisconsin-Madison.

AERI / NIST Reference Blackbody Comparison
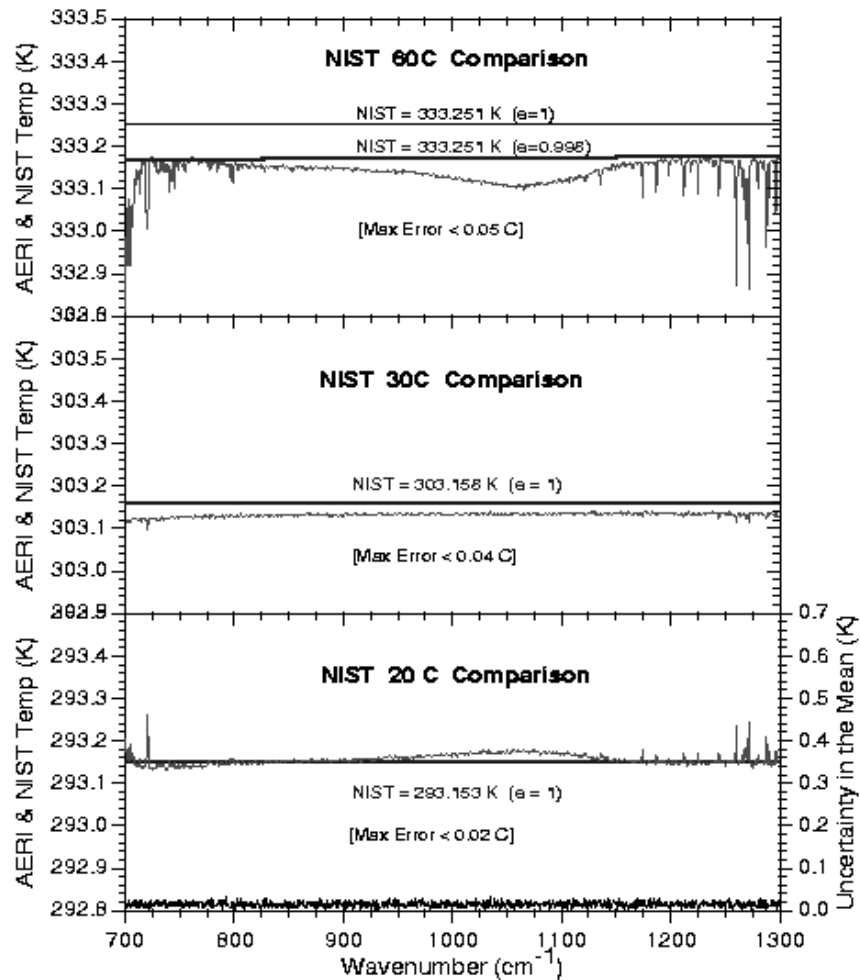
Miami IR Workshop 2-4 March 1998

Figure 17. Spectra of the M-AERI 02 and NIST black-body temperatures for three sets of measurements at 20°C, 30°C and 60°C. In the field, the M-AERI skin SSTs are derived from measurements taken at the wavenumber interval of 1302.0 to 1307.0 cm⁻¹.

Bulk SST measurements are made during the cruises using ship-mounted thermo-salinograph systems, with the intake typically at a depth of about 5m. When the ships are on station, or progressing at a few knots, bulk SST can be measured by a precision thermistor (YSI model 44032) mounted in a float so that the thermometer is in undisturbed water, ahead of the ship's bow wave, at a depth of 2-5 cm. In the cases discussed here, the float is formed from a foam-filled hard hat.

Table 13. Details on the ship-board instrumentation.

Variable	Sensor	Comments
Skin Sea Surface Temperature	M-AERI	Continuous measurements
Near surface bulk SST	Surface float	Only with ship on station
Bulk SST	Ship's thermo-salinograph	Continuous measurements
Air Temperature*	Thermistor	Continuous measurements
Relative humidity*	Vaisala "Humicap"	Continuous measurements
Wind speed*	R. M. Young anemometer	Continuous measurements
Wind direction*	R. M. Young anemometer	Continuous measurements
Barometric pressure*	Digital barometer	Continuous measurements
Insolation* (SW↓)	Eppley pyranometer†	Continuous measurements Sensors gimbaled to compensate for ship's motion.
Incident thermal radiation (LW↓)	Eppley pyrgeometer†	Continuous measurements Sensors gimbaled to compensate for ship's motion.
Cloud type and cover	All-sky camera	Continuous measurements
Atmospheric humidity profiles	Radiosondes	Up to a few per day
Atmospheric temperature profiles	Radiosondes	Up to a few per day

*Part of Coastal Environmental System's "Weatherpak"

Profiles of atmospheric temperature and relative humidity are take using a Vaisala PP15 radiosonde system. The ascent, which usually reaches pressures of 50hPa or less (*i.e.* altitudes of 20km or more) take between one and two hours to complete. When possible, we attempt to have the radiosonde ascent in progress at the time of the satellite overpass. These profiles are used to characterize the atmospheric conditions in which the M-AERI and satellite data are taken, and also with the RAL radiative transfer model to simulate the top-of-atmosphere emitted radiance spectra.
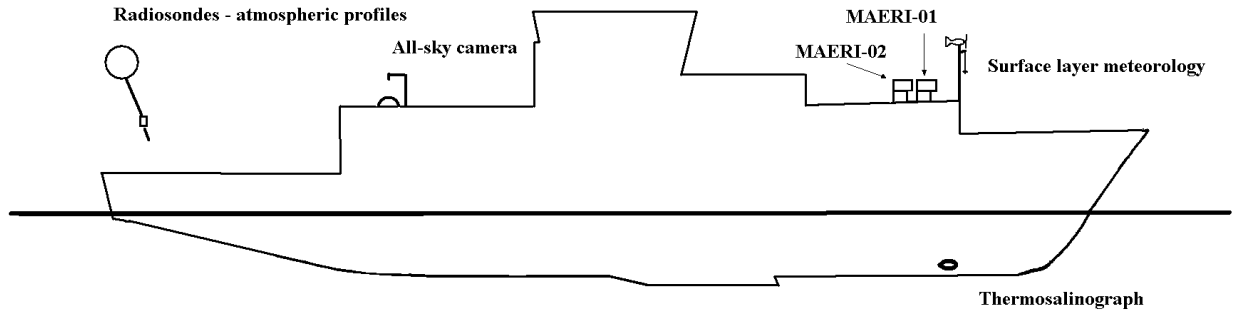
Figure 18. Schematic diagram of the instruments placed on the R/V *Roger Revelle.*

Two new instruments are currently being added to this suite to provide additional measurements to more completely characterize the conditions.

- As discussed above, aerosols are a significant source of error in satellite SST measurements. To provide measurements from which aerosol properties can be derived, a new radiometer has been added to the sea-going instruments. This is a "Portable Radiation Package" (PRP), an instrument developed at Brookhaven National Laboratory. The heart of the instrument is a fast-rotating shadowband radiometer, an enhancement of land-based Multi-Frequency Rotating Shadowband Radiometer [Harrison *et al.*,1994], modified to enable use at sea. Measurements are made in the visible part of the spectrum in 10 nm-wide bands centered at 412, 500, 615, 673, 870 and 940 nm, and in a broadband channel from 410 to 1000 nm. An occluding hemispheric arm circles the sensor head every ~6 s, casting a shadow over the aperture for a fraction of a second. Two-hundred and fifty samples from each channel are taken during the upper hemisphere transit of the arm and from these the on-board processor derives statistics for the period of each sweep. All individual data are stored and post analyzed into two-minute estimates of global, diffuse, and direct beam irradiances; aerosol optical depths are subsequently derived [Harrison and Michalsky, 1994]. At the time of writing the instrument is deployed on the USCGC *Polar Sea* (see below), and the data have not yet been analyzed.
- The second new instrument, currently being tested at RSMAS, is an optical rain gauge, which will measure precipitation at sea. Theoretical studies indicate the disruption of the skin layer by falling rain, and the subsequent modification of the static stability of the surface skin layer by the resultant drop in salinity, may both have a significant influence on the formation and maintenance of the skin-layer temperature gradients [Schlussel *et al.*, 1997; Craeye and Schlussel 1998].

54

4.3.3 M-AERI expeditions

The pre-launch M-AERI cruises (figure 13) are listed in Table 14. These have provided
   a) valuable experience in using the instruments at sea;
   b) the basis for improvements in the hardware, operating software and analysis software;
   c) measurements for the study of the surface skin layer properties, and
   d) data for a validation exercise using AVHRR data[4]

Table 14. Pre-launch M-AERI cruises

Project	Ship	Start date	Start port	End date	End Port	Instrument	Comments
	R/V Pelican	15 Jan. 1995	LUMCON	17 Jan. 1995	LUMCON	Proof of Concept	See Smith et al, 1996
Combined Sensor Cruise	NOAA S Discoverer	14 March 1996	Pago-Pago, American Samoa	13 April 1996	Honolulu, HI	Prototype	About 10 days spent off Manus, PNG in middle of cruise. See Post et al, 1998
Hawaii - New Zealand Transect	R/V Roger Revelle	28 Sept. 1997	Honolulu, HI	14 October 1997	Lyttleton, NZ	MAERI-1 & MAERI-2	Simultaneous use of two M-AERIs
OACES 24 N Section	NOAA S Ronald H. Brown	8 January 1998	Miami, FL	24 February 1998	Miami, FL	MAERI-1	In port in Las Palmas, Canary Islands. January 21-23.
NOW 98	CCGS Pierre Radisson	26 March 1998	Quebec City, Canada	28 July 1998	Nanisivic, Canada	MAERI-2	Data from March 28 to July 22
OACES Gasex-98	NOAA S Ronald H. Brown	2 May 1998	Miami, FL	7 July 1998	Miami, FL	MAERI-1	In port in Lisbon, May 20-25; Ponta Delgada, June 26-28
Panama Transit	NOAA S Ronald H. Brown	12 July 1998	Miami, FL	27July 1998	Newport, OR	MAERI-1	Through Panama Canal.
PACS-Mooring recovery	R/V Melville	8 Sept. 1998	San Diego, CA	29 Sept. 1998	San Diego, CA	MAERI-1	To TAO mooring line at 125°W
Western Pacific Transect	USCGC Polar Sea	5 Mar 1999	Adelaide, Australia	12 May 1999	Seattle, WA	MAERI-2	
Nauru 99	R/V Mirai	8 June 99	Yokohama Japan	20 July 99	Sikene-hama, Japan	MAERI-1	June 17 - Mirai arrives at Nauru. July 5 - Mirai departs Nauru.

The instrument and software improvements have been incremental over the period of the cruises and, with the exception of a totally weatherproof enclosure (which is the subject of current work), are all implemented in time for the first MODIS validation deployment.

In the following threes sections we describe some of the findings derived from the cruises relating the skin SST measurements to the in situ temperatures, and the results of the comparison of M-AERI skin SST with AVHRR SST retrievals.

4.3.4 Thermal skin effect

The latitudinal section of surface temperature measured by the ship (bulk) and M–AERI–01 (skin) is shown in Figure 19, upper panel. The difference between the skin and bulk temperatures is given in the lower panel together with a key for the color coding that is for the local time of the measurement. It can be seen that in nearly all cases the skin temperature is cooler than the bulk measurements, as is to be expected. Those cases where the reverse is true tend to be in the local afternoons in situations of low wind speed and are indicative of the presence of a diurnal thermocline which raises the in-situ temperature just below the sea surface to values much higher than at the depth of the ship measurement. Even the presence of a cool skin leaves the skin temperature warmer than the bulk temperature measured by the ship's system. Similar diurnal effects are to be seen in the data on other days, even in the trade winds' region although the amplitude is sufficiently reduced so that the skin-bulk temperature difference does not change sign. Nevertheless, there remains a diurnal modulation of the skin-bulk temperature difference with a peak-to-peak value of O(0.1K).

A scatter-plot of the measured skin temperature difference against measured surface wind speed (corrected for the ship's motion) reveals an envelope of points that becomes narrower with increasing wind speed (Fig. 20). The color coding in this figure indicates the local sun time of the measurements, and it can be seen at low wind speeds a widening of the distribution include positive values during the afternoon. This is the effect of the generation of a diurnal thermocline in the top few meters of the ocean, which makes the skin temperature appear to be warmer than the 5m bulk measurements. In reality, the skin remains cooler than the bulk measurement at a depth of a few centimeters. During the night, and for higher wind speeds the skin is about 0.2K± 0.2K cooler than the bulk temperature.
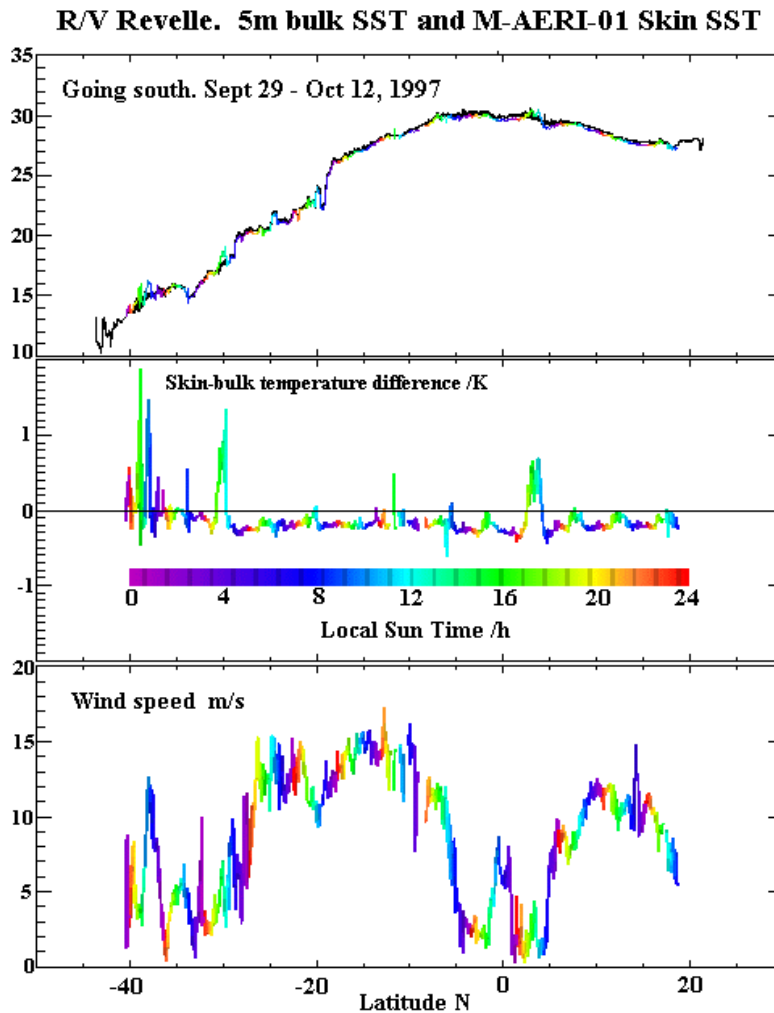
Figure 19. Latitudinal section of surface temperature measured at 5m depth (bulk) shown as black, and by the M-AERI (skin) color coded according to the time of measurement from Hawaii to New Zealand (top). The difference between the skin and bulk temperatures is shown in the middle panel with the color code showing local sun time. Wind speed, corrected for the effects of ship motion, is shown in the lower panel using the same color coding.

A similar analysis using components of the turbulent fluxes, and the next heat flux, did not yield such a clear-cut dependence. This is presumed to be the result of larger uncertainties in the flux estimates obscuring the dependences rather than a demonstration that such dependences are absent.
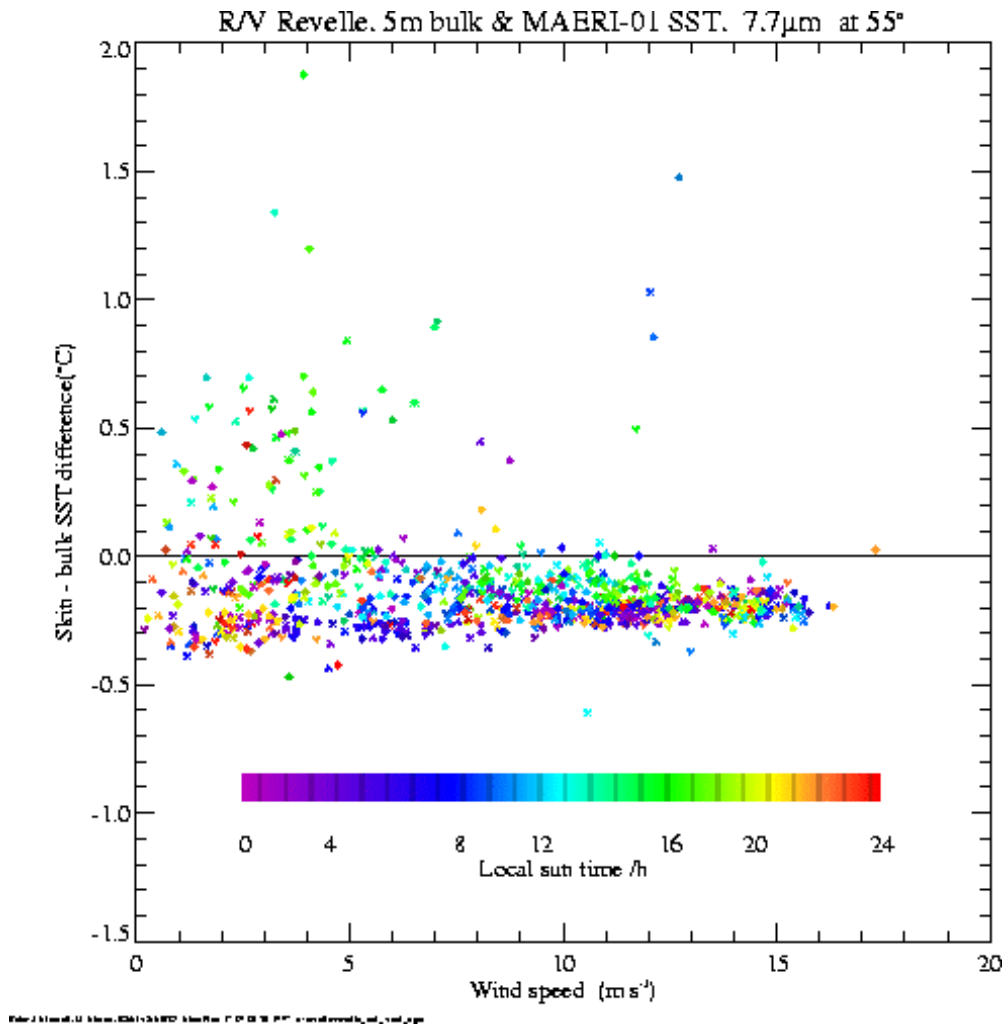
Figure 20. Wind speed dependence of the skin-bulk temperature difference measured on the R/V *Roger Revelle* cruise from Hawaii to New Zealand.

4.3.5 Diurnal thermocline effects

Figure 21 shows independent measurements of sea surface temperature taken at a station in the Tropical Western Pacific from the *NOAA S Discoverer*. The thin line that makes excursions for high temperatures is an *in situ* measurement taken from a float at a depth of ~0.1m; the dark line that does not reach high temperatures is an *in situ* measurement at 5m depth. The two other lines are skin temperature measurements taken by the M-AERI at the infrared wavelengths shown at 55° zenith angle. The wind was very light during the day (local time is UTC+9.5h) and a strong diurnal thermocline built up during the day. At night this was eroded by convective mixing and the two *in situ* temperatures converge. During both night and day the skin temperature is cooler

58

by up to a few tenths of a degree, but the afternoon measurements can be interpreted in terms of an <u>apparent</u> warm skin layer, which is simply the result of not resolving the vertical temperature gradients between the depth of the *in situ* sensor and the sea surface. This explains the results above and published in the literature (*e.g.* Cornillon and Stramma, 1985]. While the diurnal thermocline in this example is rather extreme, the skin gradients are typical, illustrating the need to include them in the validation of MODIS SST products.
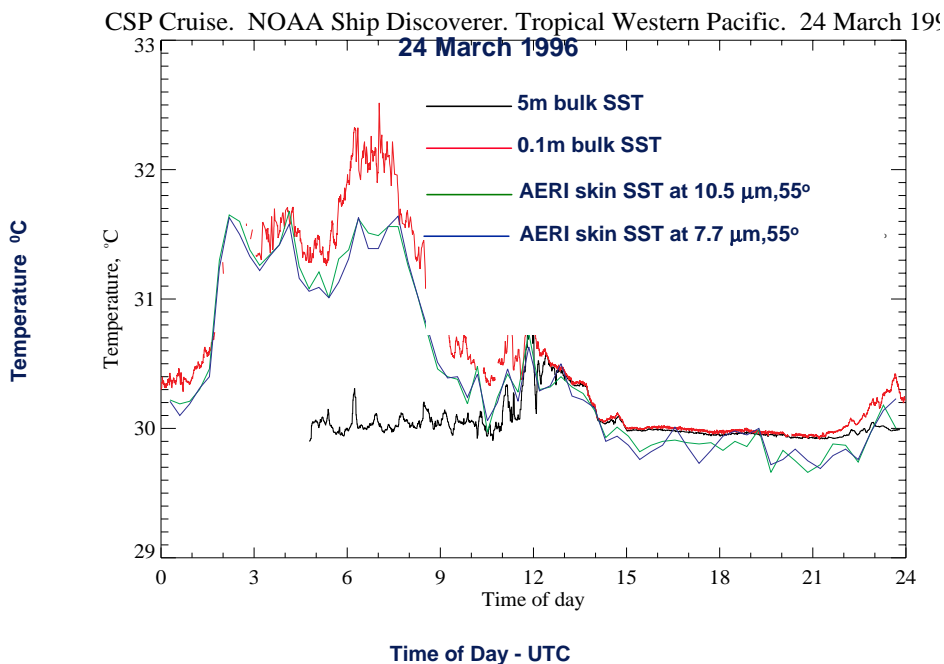
Figure 21. Time series of the M-AERI skin SST (derived at two wavelengths), and two in situ temperatures. The data were taken of Papua New Guinea in the Tropical Western Pacific Warm Pool, during the Combined Sensor Cruise of the NOAA S Discoverer.

4.3.6 SST validation using AVHRR

The skin SSTs derived form the M-AERI measurements have been compared with AVHRR SSTs derived using the Miami AVHRR Pathfinder algorithm (see above, and the ATBD of Dr. R.H. Evans) as a practice exercise prior to MODIS validation. Both the M-AERI and AVHRR data were subject to quality controls prior to producing a matchup dataset. Ideally the quality control of each data stream (M-AERI and AVHRR Pathfinder SSTs) should be independent and the two data streams only brought together for the comparison itself. However, in this case we know there are issues at

play that can introduce errors in to the data that are not attributable to the clear sky atmospheric correction algorithm. For the AVHRR these are sub-pixel cloud and instrumental effects, such as digitizer errors; for the M-AERI these are undetected spray or other contamination of the field of view, or, very rarely, as-yet undetermined measurement or data transmission errors that may be radio frequency interference. Given that extensive comparisons between the AVHRR Pathfinder SST and *in situ* measurements from drifting buoys indicate the expected uncertainties in the comparison, attributed to the AVHRR Pathfinder algorithm, are about 0.5K rms (1σ) about a mean <0.1K, we feel justified in using tests in the M-AERI quality assurance that include rejection of outliers based on a comparison between M-AERI data and the Reynolds' AVHRR-based OISST (Optimally Interpolated SST; Reynolds and Marisco,1993). The first step in the M-AERI quality control is removing all measurements taken when the aperture was covered. Then M-AERI data were eliminated that were more than ±3K from the Reynolds' OISST. Also, those M-AERI SST values were removed that differed from the coincident ship's thermosalinograph measurements (where available) by more than given thresholds, which were determined from the R/V *Revelle* deployment (figure 20). The difference, ΔT, between the skin and the bulk temperatures under a range of typical wind and sea conditions were found to be -1.75K < ΔT < 0.5K. Finally, the standard deviation of each M-AERI air temperature[5] and SST retrieval (determined from the variability of the individual M-AERI interferograms used to produce each spectrum) were used to eliminate those measurements where the standard deviation of the air temperature estimate exceeded 0.06K or that of the sea surface temperature estimate exceeded 0.09K. For the AVHRR data, the quality assurance tests developed for the Pathfinder – buoy match ups were applied (see section 5 below, and the ATBD of Dr. R.H. Evans).

The M-AERI locations and times from the cruises listed in Table 15 were used to identify those AVHRR orbits that would provide data coincident and collocated with the M-AERI. The AVHRR Pathfinder SSTs were mapped at 4 km resolution. For each mapped orbital scene pixels within 4 km and 90 minutes to the M-AERI measurement were extracted. In some cases an AVHRR pixel may be compared with more than one M-AERI SST.

---

[5] By analyzing measurements taken in spectral intervals where the atmosphere is not very transmissive, the air temperature near the ship can be derived.

Table 15. M-AERI –AVHRR Match-up cruise times and locations.

Cruise Name	Ship	Year	Begin Day	End Day	Area of Study
Combined Sensor Program (CSP)	NOAA S *Discoverer*	1996	78	103	Equatorial Western Pacific
Hawaii-New Zealand transect (HNZ)	R/V *Roger Revelle*	1997	272	286	Central Pacific Meridional Section
Section 24°N Section (24N)	NOAA S *Ronald H. Brown*	1998	8	55	Zonal Section along 24 °N in North Atlantic
GASEX (GSX)	NOAA S *Ronald H. Brown*	1998	127	188	Mid-latitude North Atlantic
Florida- Panama- Oregon Transit (FPO)	NOAA S *Ronald H. Brown*	1998	196	210	Florida to Panama to Oregon
North Water Polynya study (NOW)	CCGS *Pierre Radisson*	1998	150	203	Baffin Bay, Arctic Polynya

Some ancillary information was also assembled to aid in the interpretation of the comparison. To provide an independent estimate of the atmospheric water vapor content at each AVHRR pixel selected for the match-up, daily Special Sensor Microwave Imager (SSM/I) water vapor values were obtained by spatial bilinear interpolation to its location. The thermo-salinograph (TSG) data, with SST computed every 30 seconds, provide a bulk estimate of the SST for each cruise (see figures 20, 21 and 22). For the NOW98 cruise, these TSG data have not yet been released by the Japanese group doing the quality assurance, necessitating that some statistics be given inclusive and exclusive of this cruise. The values of the weekly Reynolds' OISST were also extracted for each target pixel using bilinear interpolation from the 1° fields; these values are compared to M-AERI SST along the whole cruise track. The assembly of these other SST estimates for comparison with the M-AERI measurements allows the M-AERI—Pathfinder comparisons to be placed in a more familiar context.

The SST from the M-AERI—Pathfinder points from the 1998 GASEX cruise are plotted in Figure 22, which also gives the time and location of the M-AERI—Pathfinder points, as well as the continuous records from the TSG and interpolated values from the OISST.
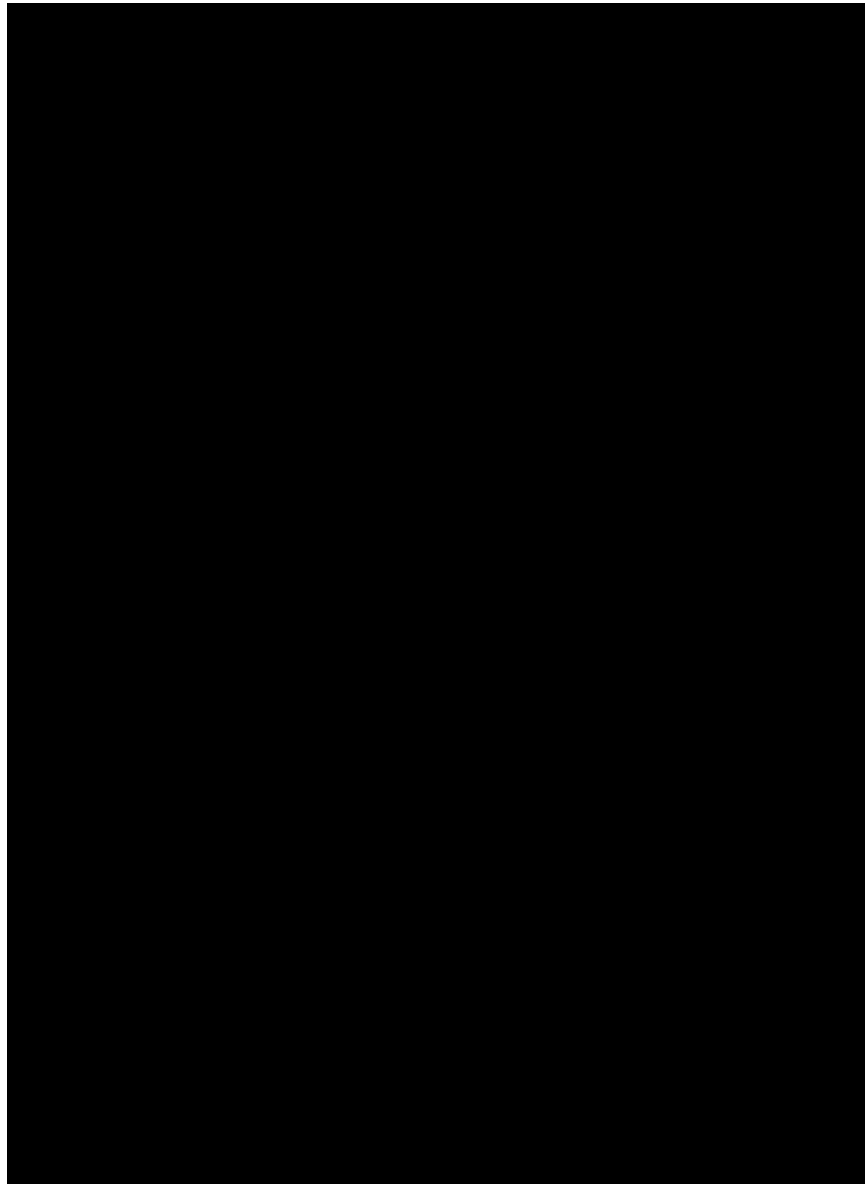
Figure 22. The cruise track and day of year [top], continuous MAERI (red), TSG (orange), and OISST (green) sea surface temperature estimates [middle], and the differences between the TSG, OISST, and Pathfinder (blue) SST estimates and the skin temperature measured by MAERI [bottom] for the 1998 GASEX cruise.

The sparcity of the M-AERI—Pathfinder matchups, compared to the M-AERI—TSG and M-AERI—OISST data, is apparent. This is because, away form the high latitude regions, each NOAA polar orbiting satellite passes overhead only twice a day, and at those times it is necessary for the M-AERI to be in a location of clear skies to register as a good M-AERI—Pathfinder comparison.

The statistics of the results from the SST, using the M-AERI SST as the reference temperature, from each cruise and as a whole, are presented in Table 16 and are depicted graphically in Figure 22. Note that the mean difference, combining all good records from the mid-latitude cruises, between the Pathfinder and the M-AERI SSTs is 0.06K, with a standard deviation of 0.29K. Inclusion of the noisier NOW data increase these estimates to 0.13 ± 0.37K. The results are biased towards those from the GASEX98 and NOW98 cruises, as the data collected during these are more numerous than those from other shorter cruises.

Table 16. Summary Statistics for M-AERI Matchups.

Cruise Description	SST Difference	Mean	Standard Deviation
CSP 1996, N = 23 (1112 total)	TSG - M-AERI	0.07 (0.04)	0.10 (0.20)
	OISST - M-AERI	0.20 (0.09)	0.32 (0.45)
	MPFSST- M-AERI	0.16	0.20
HNZ 1997, N = 6 (726 total)	TSG - M-AERI	0.10 (0.14)	0.05 (0.19)
	OISST - M-AERI	0.04 (-0.13)	0.08 (0.49)
	MPFSST- M-AERI	-0.03	0.25
24N 1998, N = 16 (1833 total)	TSG - M-AERI	0.22 (0.17)	0.07 (0.13)
	OISST - M-AERI	0.05 (0.08)	0.42 (0.41)
	MPFSST- M-AERI	0.03	0.18
GASEX 1998, N = 168 (5104 total)	TSG - M-AERI	0.02 (0.02)	0.30 (0.32)
	OISST - M-AERI	0.32 (0.30)	0.47 (0.56)
	MPFSST- M-AERI	-0.01	0.25
FPO 1998, N = 47 (1244 total)	TSG - M-AERI	0.14 (0.06)	0.19 (0.29)
	OISST - M-AERI	0.85 (0.37)	0.86 (0.71)
	MPFSST- M-AERI	0.27	0.40
NOW 1998 (Arctic), N = 176 (4251 total)	TSG - M-AERI	NA (NA)	NA (NA)
	OISST - M-AERI	-0.79 (-1.11)	0.57 (0.82)
	MPFSST- M-AERI	0.24	0.44
Total, all data, N = 436 (total 14277)	OISST - M-AERI	-0.08 (-0.18)	0.82 (0.89)
	MPFSST - M-AERI	0.13	0.37
Total, excluding NOW data, N = 260 (total 10015)	TSG - M-AERI	0.06 (0.06)	0.26 (0.28)
	OISST - M-AERI	0.38 (0.21)	0.58 (0.56)
	MPFSST- M-AERI	0.06	0.29

The numbers in brackets refer to statistics derived from all appropriate data and not just restricted to the times of match-ups with the AVHRR.
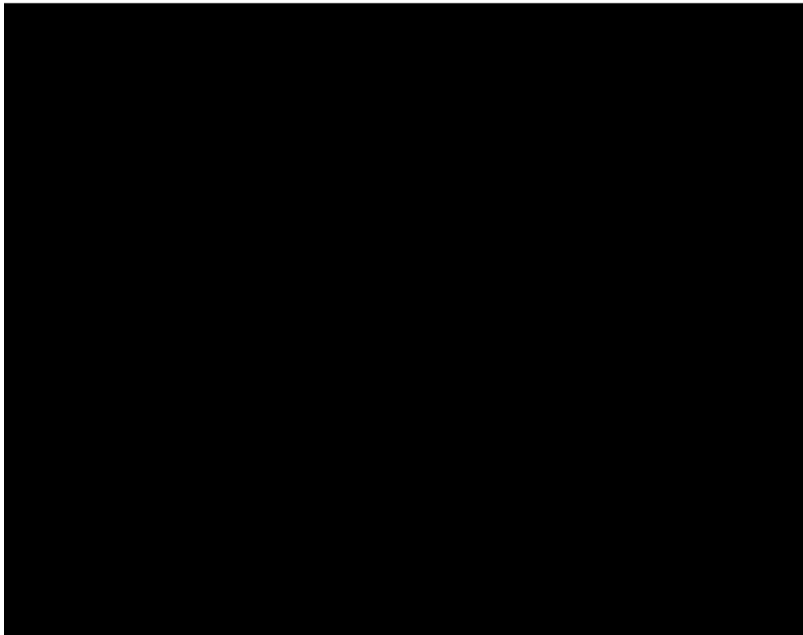
Figure 23 The mean (abscissa) and standard deviation (ordinate) of the difference of the various SST estimates from the reference MAERI SST. The cruise abbreviation (see Table 15) is centered on the point with the number of observations for that cruise appearing as a subscript.

These results compare very favorably with those from the climatological study of Casey and Cornillon [1999] and with the estimates from a similar, much more extensive, comparison of NOAA-14 MPFSST to buoy data which provides a mean difference of 0.02 K and a standard deviation of 0.53K. The ships' TSGs are closest to the M-AERI SST; those times where there are substantial differences are related to skin—bulk SST differences at times of high insolation and small wind mixing. Next best is the Pathfinder 4 km resolution estimate, generally >10% worse than the TSG with an additional bias of approximately 0.5K. The Reynolds' OISSTs have the largest errors, which is not surprising given the weekly averaging and smoothing inherent in those fields. The OISST outliers are the result of poor OISST boundary conditions in the Arctic (NOW) and along the west coast of North America (FPO).

Given the small size of the current M-AERI dataset, the accurate portrayal of the effects of clouds, water vapor, and aerosols on the Pathfinder SST retrievals will have to wait for future M-AERI deployments in a greater range of atmospheric conditions. Nevertheless it is instructive to show a few of these relationships. Figure 24 shows the effect of water vapor for oblique scan angles. While all points are considered high

64

quality with regard to the pixels' homogeneity, the Pathfinder—M-AERI difference versus the SSM/I water vapor estimate suggests a tendency for the large zenith angle (>45°) to underestimate the SST with increasing integrated water vapor content. While there are not enough independent data to accurately model this relationship in this study, this effect has also been noted by [Kumar *et al.*, 1999].

Figure 24 The relationship between water vapor content as estimated from the SSM/I instrument versus the Pathfinder-MAERI difference for 'quality level 7' pixels [top panel] and 'quality level 6' pixels [bottom]. The level 6 pixels differ from the level 7 pixels only in that they are derived from observations with an oblique (>45°) viewing angle. An oblique viewing angle leads to a longer path length through the atmosphere which makes the SST estimate more susceptible to the effects of atmospheric water vapor, resulting in a trend towards negative residuals with increasing water vapor for the level 6 pixels. The numbers in the plots are keyed to the cruises as follows: 1=CSP, 2=HNZ, 3=24N, 4=GSX, 5=FPO, 6=NOW (see Table 15).

The results of the comparisons from the Arctic NOW98 cruise have enhanced error for a number of reasons. The lack of the TSG data and a meaningful Reynolds' OISST field hindered the M-AERI quality control as outliers are more difficult to identify. More importantly, the Pathfinder algorithm may not perform well in the Arctic due to a lack of in situ buoy data with which to calculate the appropriate Pathfinder coefficients, a

poor first guess field provided by the Reynolds' OISST average, and the nearby presence of sea ice may adversely affect the AVHRR retrievals.

Although the number of M-AERI—Pathfinder points is relatively small, these results suggest that the Miami Pathfinder algorithm is much more accurate than has been estimated by previous studies - at least for those atmospheric and oceanic conditions sampled by these six cruises. The fact that Pathfinder SSTs are nearly as good as the thermosalinographs of these research vessels, when compared to the M-AERI data, is very encouraging for global SST studies using AVHRR data. The similarity of the Pathfinder and TSG statistics confirms that the Pathfinder algorithm derives an estimate of a bulk temperature in which a mean thermal skin effect is embedded, as a direct result of the method of deriving the coefficients. The larger error exhibited by the Reynolds' OISST fields gives a good indication of the minimum temperature difference necessary for meaningful interpretation of that difference when making Pathfinder SST *vs* Reynolds' OISST comparisons, which is often done since the Reynolds' fields are global and are easily available.

The M-AERI—Pathfinder comparisons have clearly demonstrated the feasibility of using M-AERI measurements to validate the MODIS SST retrievals.

4.3.7 Operational surface networks

Selected radiosoundings from the operational network of meteorological observing stations will be used to define the global distributions of the atmospheric temperature and water vapor profiles for use in MODIS infrared band simulations for the development of the atmospheric correction algorithm.

Measurements from the operational surface drifting and fixed buoy programs will be used to characterize the surface temperature fields and to validate the atmospheric correction algorithms used with data from the AVHRR (Advanced Very High Resolution Radiometer) as in the fashion developed for the AVHRR SST Pathfinder program.

The assimilated meteorological fields produced by operational weather services (National Meteorological Center, European Centre for Medium-Range Weather Forecasting) provide a valuable description of the marine atmosphere and surface (strictly sub-surface bulk) sea temperature. These fields will be used in conjunction

with the radiative transfer modeling to simulate the MODIS measurements, initially to give confidence that the selection of radiosoundings used to characterize the marine atmosphere is indeed representative, and, subsequently, if it can be shown that the assimilated fields are of sufficiently high accuracy, to provide direct input to the radiative transfer modeling.

4.3.8 ATSR data

The ATSR (Along Track Scanning Radiometer - Edwards *et al.*, 1990; Minnett, 1995a & 1995b) Project in the UK has recently delivered the corresponding ATSR data to us. These will be used in a comparable study to that described above for AVHRR. The ATSR long-wave channels match quite well the spectral characteristics of the MODIS long-wave bands (31 and 32), and the noise characteristics of the ATSR channels are very good [Minnett, 1995b]. The ATSR series are radiometers that are very well characterized before launch and have two internal black-body targets for in-flight calibration [Armitage *et al.*, 1990; Minnett 1985b]. Like the AVHRR, the ATSR has a single channel in the 3.5 - 4.0 µm window and so cannot supply comparable data to those expected form MODIS bands 20, 22 and 23.

4.4 Post-launch activities

The initial post-launch activities will focus on gathering surface and atmospheric data that are collocated and contemporaneous with the MODIS measurements.

4.4.1 M-AERI field campaigns

Given a launch in late July 1999, and a period of ~30 days for spacecraft operations before the MODIS infrared data begin being transmitted to earth, we anticipate the data flow to start in September 1999. In the following three months we have planned four cruises in climatologically diverse conditions, ranging from the Arctic to the Tropical Atlantic Ocean (table 17; see also figure 13). Further cruises for the duration of the MODIS missions will be undertaken to generate the large dataset necessary for a thorough validation of the MODIS SST retrievals.

It is anticipated that some of the future validation campaigns will be centered on the DOE ARM sites in the TWP and the NSA-AOO where the instrumentation installed there will provide an unparalleled description of the state of the atmosphere. As part of the ARM operations, periodic Intensive Operations Periods [Stokes and Schwartz, 1994;

Mather *et al.*, 1998] are undertaken during which the sampling frequency and is increased and additional, often experimental instruments, are deployed. Particular attention will be paid to the possibility of coordinating MODIS validation with ARM activities during these periods.

Table 17. Planned post-launch M-AERI deployments 1999

Project name	Ship	Departure Date	Departure Port	Arrival Date	Arrival Port	Comments
NOW 99	CCGS Pierre Radisson	24 August 99	Quebec City	~10 October 99	Quebec City	Study area is the North Water Polynya between northern Greenland and Ellesemere Is.
MODIS Initialization	R/V Melville	1 October 1999	San Diego	20 October 1999	San Diego	Off Baja California. Joint with MODIS Ocean Color group.
Straits of Sicily	R/V Urania	15 October 1999	TBD	15 Nov. 1999	TBD	Collaboration with Institute of Atmospheric Physics, Rome. May experience N. African dust over Mediterranean.
Eastern Atlantic Transect	R/V Polarstern	15 December 1999	Bermerhaven, Germany	6 January 2000	Cape Town. South Africa	Will transit Saharan aerosol outflow region

Cruises of opportunity, such as those associated with the MOBY and the possible supplementary ARM ocean sites, will be exploited wherever possible. Another exciting possibility is to mount an M-AERI on one of the Antarctic research support vessels on their transoceanic cruises to or from Antarctica. US Coast Guard ice-breakers sail from Seattle to Antarctica each year, and an ice-strengthened research ship of the British Antarctic Survey makes comparable voyages in the Atlantic Ocean. Also negotiations are underway to mount a M-AERI and ancillary instruments on a new, very large cruise liner being built be Royal Caribbean, which would provide a year-round data set in the Caribbean, western Atlantic Ocean area. In addition, it is anticipated that the M-AERI will be deployed on fixed research platforms during the MODIS lifetimes.

4.4.2 Aircraft campaigns

Low-flying aircraft provide alternative platforms for the validating radiometers, and aircraft can seek out the clear air conditions, avoiding the clouds that obscure the

position of fixed or slowly moving ships at the times of satellite overpasses on a significant number of occasions. Collaborations will be forged with groups using HIS-type instruments on aircraft that can fly low (h<50m) over the ocean.

Broad band infrared radiometers, if proven to be beneficial during the pre-launch studies, will be used on ships of opportunity as these arise.

4.4.3 Collaboration with other groups

In collaboration with the MODIS Atmospheric group, high-flying aircraft campaigns will be utilized, when their planned flights include segments over the ocean.

Comparisons between MODIS SST fields and measurements from analysis of fixed and drifting surface buoys will be continued throughout the MODIS missions to provide long-term monitoring of the performance of the SST algorithm and data for progressive algorithm refinement. This is dealt with in more detail in section 5.

Several aircraft campaigns of the MODIS Atmospheric Group are planned to be made over mid-latitude oceanic areas in the first few years of MODIS operations. These will be used to validate the MODIS top-of-atmosphere radiance measurements and SST retrievals. At present it is not clear what research cruises will be being undertaken in the post-launch period, but efforts will be made to coordinate MODIS infrared validation exercises with those that offer promising opportunities.

4.4.4 Needs for other satellite data

Inter-satellite comparisons can be done on an opportunistic basis throughout the mission, provided suitable validating instruments on other satellites (table 18).

In the period of the first few years of the of the AM-1 mission, possible validating instruments are the Advanced Very High Resolution Radiometer on the NOAA satellites, the Along-Track Scanning Radiometer (ATSR) on the ERS-2 satellite, or the Advanced ATSR (AATSR) on the European Polar Platform of the Envisat-1 Mission, scheduled for launch in –late 2000 [Cendral, 1995], the second Ocean Color and Temperature Scanner (OCTS-II) and the Global Imager (GLI) on the Japanese ADEOS-II satellite. All of these instruments have a spatial resolution of 1km at nadir, with the exception of OCTS-II, which has a spatial resolution of 0.7km.

Table 18. Band characteristics of satellite-borne infrared radiometers

	MODIS[1]		AVHRR[2]		ATSR[3]		OCTS[4]		GLI[5]	
NO.	λ (μm)	NEΔT (K)	λ (μm)	NEΔT (K)	λ (μm)	NEΔT (K)	λ (μm)	NEΔT (K)	λ (μm)	NEΔT (K)
20	3.75	0.05	3.75	0.12	3.7	0.019	3.7	0.15	3.715	<0.15
22	3.96	0.05								
23	4.05	0.05								
29	8.55	0.05					8.52	0.15	8.3	<0.1
31	11.03	0.04	10.5	0.12	10.8	0.028	10.8	0.15	10.8	<0.1
32	12.02	0.04	11.5	0.12	12.	0.025	11.9	0.15	12	<0.1

[1] For Proto-Flight Model. From graphic presented by T. Pagano at MODIS Science Team Meeting, November 1995.

[2] For a target temperature of 300K [Planet, 1988].

[3] Derived from 500 samples of black-body measurement at a temperature of 298K [Minnett, 1995b]. The infrared spectral and radiometric characteristics of AATSR are expected to be comparable.

[4] For a target temperature of 300K. From OCTS instrument description.

[5] From NASDA Research Announcement , October 24, 1995.

4.4.5 Measurement needs (*in situ*) at calibration/validation sites

Validation sites will be selected where the ancillary measurements needed to specify the atmospheric state, such as at the ARM sites (see above). At this stage it is not possible to foresee whether the instrumentation suites at these site will need augmentation. If broad-band infrared radiometers can be shown to provide SST measurements of sufficient reliability to validate the MODIS retrievals, and if these are deployed on ships of opportunity, it may be necessary to augment the instruments on these ships to provide the necessary ancillary measurements, such as radiosondes and a sky camera. Similarly, when the M-AERI is deployed on fixed platforms, it is likely that additional instruments will be needed to provide the atmospheric measurements.

The spatial distribution of the set of the operational free-drifting buoys may not be ideal for the long-term validation of the MODIS SST retrievals, in which case it will be necessary to seed particular ocean areas that are critical to the validation, but are inadequately sampled by the buoys in place at that time.

4.4.6 Needs for instrument development

The continuing development of the M-AERI is anticipated to provide a reliable and accurate primary validation instrument throughout the periods of the MODIS missions.

A number of other groups in the US, Europe and Australia are developing and using broad-band infrared radiometers. Some are planned for deployment on ships of opportunity. It is likely that it may be necessary to develop *in situ* calibration equipment to improve the long-term stability and accuracy of these measurements.

4.4.7 Geometric registration site

It is not anticipated that such a facility will be needed for the MODIS infrared band validation over the oceans.

4.4.8 Intercomparisons (Multi-instrument)

Intercomparison with other satellite instruments will be primarily with instruments on other platforms (see 4.4.5). Comparisons are planned with the ASTER instruments to use their high spatial resolution to explore the influences of sub-pixel features, such as small clouds, or the MODIS Sea-Surface temperature retrievals. Discussions have been held with the ASTER group at JPL to coordinate validation activities, and requests have been made for high-resolution ASTER data over the ocean for comparison with MODIS measurements.   The MODIS aerosol products, derived by the Ocean Color Group (Howard Gordon) and the Atmospheric Group (Yoram Kaufman, Didier Tanré) are expected to be of use in determining the causes of the residual errors in the MODIS SST retrievals.

4.5   Implementation of validation results in data production

4.5.1 Approach

The algorithm for SST derivation from the MODIS infrared measurements has been delivered. To provide a consistent output data stream, it is important that the data production algorithm not be adjusted frequently, and when it is revised the changes must be well recorded in the metadata associated with the product. It is anticipated that for the first 12-24 months after launch, the validation data will be analyzed in a 'research' mode and trial refinements of the algorithm will be fully tested off-line before being implemented at the processing center. It is expected that part of the algorithm refinement will incorporate findings and results from other groups, especially those that are also involved in monitoring the on-board infrared calibration process. Retrospective reprocessing of data will be done on large data segments, say of a year's

length or more, at which time it will be necessary to distribute the revised products to all users of the previous product versions.

4.5.2 Role of EOSDIS

EOSDIS will be a valuable source of data and analysis tools to be used in the algorithm refinement and in the post-launch validation activities.

4.5.3 Plans for archival of validation data

All data sets gathered or derived for the purposes of validation of the MODIS infrared bands will be made available to the scientific community through EOSDIS and the World Wide Web.

5.0 Validation using *in situ* sea surface temperature measurements

Section 4 dealt with the radiometric aspects of validating the MODIS infrared measurements over the seas. This section deals with validation activities using long time series of *in situ* sea surface temperatures derived from surface buoys. This activity builds on the experience gained in the NASA/NOAA AVHRR Ocean Pathfinder project, and will be conducted in close collaboration with the MODIS activities being led by Dr. R.H. Evans of the Rosenstiel School of Marine and Atmospheric Science.

We will characterize overall algorithm performance by assembling two comparison databases: a North American match-up database (MDB) and a Global match-up database. The North American MDB will be principally composed of surface observing sites in North American coastal waters while the global MDB will include all fixed and drifting platforms. Data availability drives generation of the two comparison datasets. Currently the North American observations are available in near real time while the global observations have delays of days to weeks associated with their retrieval.

5.1   Sources of *in situ* SSTs and other environmental variables

The environmental data used in both MDBs will be obtained from the various sources summarized in Table 19. The observations are from two main types of platforms: moored buoys and drifting buoys. The North American MDB will contain *in situ* observations only from the US National Data Buoy Center (NDBC) moored buoys located from the Gulf of Maine to the Gulf of Mexico (latitudinal range: 42.5°N to 25.9°N).

Table 19. Sources of *in situ* SST Values to be Included in the MODIS Sea_sfc Temperature Algorithm Matchup Databases

TYPE	PLATFORM	SOURCE
Moored buoys	NDBC	US National Data Buoy Center, NDBC (through NASA/GSFC)
	Japanese	Japanese Meteorological Agency
	TOGA/TAO	NOAA Pacific Meteorological and Environmental Laboratory
Drifting Buoys	AOML	NOAA Atlantic Oceanographic and Meteorological Laboratory
	MEDS	Canadian Marine Environmental Data Service (through NASA/GSFC)

Some of the in situ platforms (particularly the moored buoys) include environmental variables other than SST. The version of the Global MDB, however, will include only the following in situ quantities, which are common to all data sources:

- Buoy ID
- Latitude
- Longitude
- Time
- Sea surface temperature

On the other hand, the North American MDB will include the following additional environmental variables:

- Significant wave height
- Air temperature
- Wind speed and direction (average over the first 8 minutes of each reporting period, usually once per hour)
- Dew point temperature

5.2   MODIS Data Extractions

For both the MDBs, MODIS data will be extracted for 3x3-pixel boxes centered at each *in situ* SST location. The initial extraction data set includes only the level 1a counts, which are converted to brightness temperature in a subsequent step. We assume a navigation correction (time and attitude) is applied to ensure correct geolocation of the satellite data.

The MDBs will include coefficients that can be used to correct the various IR bands for changes in emissivity as a function of scan angle (variables em_i: see below for location in the record). These coefficients are taken from Bransom [1968] but new values derived from M-AERI measurements will be used if necessary. Emissivity-corrected values for the central pixel are also included in the MDB for the various bands (cm_i). Note that since the correction is performed on radiances, one cannot simply multiply the uncorrected temperatures by the coefficients and obtain the corrected values.

5.2.1 Time Coordinates

To facilitate the matchup process, dates and times of both the satellite and *in situ* data will be converted to a continuous time coordinate, *e.g.*, "seconds since January 1, 1981" is used in the Pathfinder analog. These values can be subtracted and then the actual date can be obtained through simple calculation.

5.3   Matchup Procedures

The *in situ* records are first temporally matched-up against the MODIS extractions. To limit variability introduced by the time separation between the two data sources, the absolute difference between the time of the *in situ* SST measurement and the time at which that location is viewed by the MODIS *(i.e.*, the matchup time window) is restricted to a maximum of ±30 minutes or ±15 minutes. *In situ* records that do not fall within the stipulated time window will be rejected.

The *in situ* records that pass the temporal matchup subsequently have to pass a spatial test. A maximum distance of 0.1° will be accepted between an *in situ* SST location and the location of the central pixel in the MODIS extraction box.

5.3.1 Filtering Records

To reduce the number of records to be handled by users of the databases, the matchups will be passed through a series of filters that eliminate records with obvious problems (for instance, gross cloud contamination). The records will be included in the MDB files only if they pass the following series of tests (the variable names used in the tests are described in Tables 20 and 21):

- Bsst (Buoy SST) ne "n/a"
- Ch31 (brightness temperature) < 35°C
- Ch32 (brightness temperature) < 35°C
- Satz (satellite zenith angle) < 62°
- Cen20 (field 13) - Cen32 (field 15) < 6K & Cen20 (field 13) - Cen32 (field 15) > -2K
- (Max31 - Min31) ≤3K & (Max32 - Min32) ≤ 3K

Table 20. Fields included in global matchup database (version 1).

Field No.	Field Description	Units	Code
1	Satellite observation time	Seconds	stime
2	Latitude of center pixel	Degrees	slat
3	Longitude of center pixel	Degrees	slon
4	Average PRT temperature	°C	prt
5	Solar zenith angle	Degrees	solz
6	Satellite zenith angle	Degrees	satz
7	Glint index	—	glnt
8	Emissivity correction, band 20/22/23	—	em20
9	Emissivity correction, band 31	—	em31
10	Emissivity correction, band 32	—	em32
11	Central value of 3x3 pixel box, band 20	°C	ch20
12	Central value of 3x3 pixel box, band 22	°C	ch22
13	Central value of 3x3 pixel box, band 23	°C	ch23
14	Central value of 3x3 pixel box, band 31	°C	ch31
15	Central value of 3x3 pixel box, band 32	°C	ch32
16	Median of 3x3 pixel box, band 20	°C	med20
17	Median of 3x3 pixel box, band 22	°C	med22
18	Median of 3x3 pixel box, band 23	°C	med23
19	Median of 3x3 pixel box, band 31	°C	med31
20	Median of 3x3 pixel box, band 32	°C	med32
21	Minimum value of 3x3 pixel box, band 20	°C	min20
22	Minimum value of 3x3 pixel box, band 22	°C	min22
23	Minimum value of 3x3 pixel box, band 23	°C	min23
24	Minimum value of 3x3 pixel box, band 31	°C	min31
25	Minimum value of 3x3 pixel box, band 32	°C	min32
26	Maximum value of 3x3 pixel box, band 20	°C	max20
27	Maximum value of 3x3 pixel box, band 22	°C	max22
28	Maximum value of 3x3 pixel box, band 23	°C	max23
29	Maximum value of 3x3 pixel box, band 31	°C	max31
30	Maximum value of 3x3 pixel box, band 32	°C	max32
31	Average value of 3x3 pixel box, band 20	°C	av20
32	Average value of 3x3 pixel box, band 22	°C	av22
33	Average value of 3x3 pixel box, band 23	°C	av23
34	Average value of 3x3 pixel box, band 31	°C	av31
35	Average value of 3x3 pixel box, band 32	°C	av32
36	PRT 1 Temperature)	°C	prt1
37	PRT 2 Temperature)	°C	prt2
38	PRT 3 Temperature } Black body monitor	°C	prt3
39	PRT 4 Temperature)	°C	prt4
40	Central value w/ emissivity correction, band 20	°C	cm20
41	Central value w/ emissivity correction, band 22	°C	cm22
42	Central value w/ emissivity correction, band 23	°C	cm23
43	Central value w/ emissivity correction, band 31	°C	cm31
44	Central value w/ emissivity correction, band 32	°C	cm32
45	Time of *in situ* observation	Seconds	btime
46	Buoy latitude	Degrees	blat
47	Buoy longitude	Degrees	blon
48	Buoy ID	—	bid
49	*In situ* SST	°C	bsst
50	Delta-SST (First-guess satellite SST minus *in situ* SST)	°C	sst1
51	Filter code (1 or 2)	—	pass

Table 21. Fields included in North American matchup database (version 1).

Field No.	Field Description	Units	Code
1	Satellite observation time	Seconds	stime
2	Latitude of center pixel	Degrees	slat
3	Longitude of center pixel	Degrees	slon
4	Average PRT temperature	°C	prt
5	Solar zenith angle	Degrees	solz
6	Satellite zenith angle	Degrees	satz
7	Glint index	—	glnt
8	Emissivity correction, band 20, 22, 23	—	em20
9	Emissivity correction, band 31	—	em31
10	Emissivity correction, band 32	—	em32
11	Central value of 3x3 pixel box, band 20	°C	ch20
12	Central value of 3x3 pixel box, band 22	°C	ch22
13	Central value of 3x3 pixel box, band 23	°C	ch23
14	Central value of 3x3 pixel box, band 31	°C	ch31
15	Central value of 3x3 pixel box, band 32	°C	ch32
16	Median of 3x3 pixel box, band 20	°C	med20
17	Median of 3x3 pixel box, band 22	°C	med22
18	Median of 3x3 pixel box, band 23	°C	med23
19	Median of 3x3 pixel box, band 31	°C	med31
20	Median of 3x3 pixel box, band 32	°C	med32
21	Minimum value of 3x3 pixel box, band 20	°C	min20
22	Minimum value of 3x3 pixel box, band 22	°C	min22
23	Minimum value of 3x3 pixel box, band 23	°C	min23
24	Minimum value of 3x3 pixel box, band 31	°C	min31
25	Minimum value of 3x3 pixel box, band 32	°C	min32
26	Maximum value of 3x3 pixel box, band 20	°C	max20
27	Maximum value of 3x3 pixel box, band 22	°C	max22
28	Maximum value of 3x3 pixel box, band 23	°C	max23
29	Maximum value of 3x3 pixel box, band 31	°C	max31
30	Maximum value of 3x3 pixel box, band 32	°C	max32
31	Average value of 3x3 pixel box, band 20	°C	av20
32	Average value of 3x3 pixel box, band 22	°C	av22
33	Average value of 3x3 pixel box, band 23	°C	av23
34	Average value of 3x3 pixel box, band 31	°C	av31
35	Average value of 3x3 pixel box, band 32	°C	av32
36	PRT 1 Temperature)	°C	prt1
37	PRT 2 Temperature)	°C	prt2
38	PRT 3 Temperature) Black body monitor	°C	prt3
39	PRT 4 Temperature)	°C	prt4
40	Central value w/emissivity correction, band 20	°C	cm20
41	Central value w/emissivity correction, band 22	°C	cm22
42	Central value w/ emissivity correction, band 23	°C	cm23
43	Central value w/ emissivity correction, band 31	°C	cm31
44	Central value w/ emissivity correction, band32	°C	cm32
45	Delta-SST (First-guess satellite SST minus *in situ* SST)	°C	sst1
46	Filter code (1 or 2)	—	pass
47	Time of *in situ* observation	Seconds	btime
48	Buoy latitude	Degrees	blat
49	Buoy longitude	Degrees	blon
50	Buoy ID	—	bid
51	Buoy air temperature	°C	bat
52	Buoy dew point temperature	°C	bdwp
53	Buoy wind speed	m/s	bwsp
54	Buoy wind direction	Degrees	bwdir
55	Buoy significant wave height	m	bswh
56	Buoy sea surface temperature	°C	bsst

A second set of tests define two categories for a "pass" index, which can serve as an initial guidance for data selection:

- If $1K \leq$ (Max31 - Min31) $< 3K$ & $1K \leq$ (Max32 - Min32) $< 3K$, then pass = 2
- If (Max31 - Min31) $< 1K$ & (Max32 - Min32) $< 1K$, then pass = 1.

The general approach is that the more restrictive criteria for the spatial homogeneity tests (*i.e.*, records with pass=1) can be used to estimate SST algorithm coefficients. The records with pass=2 can be used in evaluating algorithm performance. The "pass" code is included as the last field of the matchup record.

5.3.2 First-guess satellite-derived SST

As a further aid to initial use of the matchup data sets, a first-guess satellite SST (sst1) will be computed. The difference between this first-guess satellite SST and the *in situ* SST will be included in the MDBs. The first-guess SST will be computed using an MCSST. (The matchup databases will not actually include the first-guess satellite SST (sst1), but the difference between sst1 and the *in situ* SST).

5.4   Matchup database definition

The matchup database files will be maintained as flat ASCII files, with free-format blank-separated fields in each record. The number of fields per record is 51 for the Global MDB and 56 for the North American MDB. Missing values are denoted by "n/a". The fields included in both types of MDBs vary somewhat, as does their location in the record. The variables included in the global and the experimental MDBs are listed in Tables 20 and 21, respectively.

The first record in all the MDB files should be a header containing blank-separated short field names to be used if the records are imported into a spreadsheet or statistical package; these short names or codes are shown on the fourth columns of Tables 20 and 21. Specific details for each MDB type are also given in Tables 20 and 21.

5.5   Quality Control and Diagnostics

Quality control of the MODIS Sea_sfc Temperature algorithm fields is not necessarily easy since there currently do not exist any other sea surface temperature fields with similar spatial and temporal coverage. The only current candidate fields with requisite accuracy and coverage are the experimental ERS-1 Along Track Scanning Radiometer (*ATSR*) and the NOAA-NASA Pathfinder SST fields. While these fields have great potential for retrospective studies of MODIS Sea_sfc Temperature algorithm performance, they do not address the need for near-real time quality assessment of the product. Thus we propose four methods: 1) a running climatology computed from the product itself, 2) a lower resolution SST estimate computed from the AIRS instrument (product 2523), 3) comparisons with NOAA and NAVY SST products, and 4) space-time coherence tests.

5.5.1 Running Climatology Approach

An approach, which has been shown to be effective in the NOAA/NASA AVHRR Pathfinder work, is to compute a lagged climatology of the global SST where the lag (time) interval might be one week, two weeks, or a month. This running Global average temperature field is used at high resolution to provide first guess temperature for all pixel locations. The running climatology includes a mean value and a variance field for each location, T_C and V_C, respectively. T_C and V_C are functions of space and time, *i.e.*, T_C = T_C (x,y,t) and V_C = V_C (x,y,t). A range measure is adopted to classify data outliers. For example, the Global range measure might be $\pm$ 2σ (units of standard deviation). Data that lies within two standard deviations of Tc would be considered as a valid estimate, that is:

$$(T_C - 2\sqrt{V_C}) \leq T_S \leq (T_C + 2\sqrt{V_C}) \tag{25}$$

Maintenance of such a climatology for the MODIS SST algorithm has computing and mass storage implications. Each observing day a new climatology will be computed over the lag interval. Testing with the NOAA/NASA Pathfinder activity has demonstrated that one should keep separate day/night climatologies due to daytime skin – bulk T_s biases. Therefore, the climatology requires producing an average value and a variance for the last n days of each field every day and storing this for quality assessment use. Each field will have the characteristics shown in Table 22.

Table 22. MODIS IR SST Climatology Dataset

Parameter	Format
Average SST value	32 bit floating point
Variance estimate	32 bit floating point
Latitude	32 bit floating point
Longitude	32 bit floating point
Time	32 bit floating point

Given the data structure shown in Table 21, each day/night climatology field will require approximately 7.5 Gbytes per day, or a total of 15 Gbytes per day (3.5 x 10^8 (ocean pixels) x 20 bytes/pixel x 2 fields/day, or ~15 Gbytes/day).

5.5.2 Space/time Coherence

The previously mentioned quality assessment approaches rely on the presence of global fields for their implementation. Oceanographers typically test new observing systems by looking at sections in space or time, *i.e.*, time, space, or space/time series.

As part of the ongoing quality assessment activity, we will define a sequence of points for the production of time series, several space cuts through better *in situ* observed regions of oceanic basins, and a few specific sections for the generation of space/time diagrams. Products from this activity will facilitate quick look tests of space/time coherence.

5.6   Implications for the ECS, TLCF and MOTCF Efforts

It is unclear which facilities will generate the climatology and other quality control products. It is apparent they can be generated in the ECS or by the TLCF or by the MOTCF. We note that one of them will have to produce the various products on a routine basis.

5.7　Exception Handling

Exception handling for the Sea_sfc Temperature algorithm is straightforward. To our knowledge there is no processing condition which should 'hold' Sea_sfc temperature processing. Data quality flags will be provided for all anomalous cases. The approach is to process all available non-land infrared radiances for Sea_sfc temperature, and then flag each estimate for missing radiances, clouds, dropouts, *etc.* As is stated in the calibration-validation section, we require daily day/night global mosaics of the Sea_sfc Temperature, flag words, with compilations of numbers of each flag's occurrence. Note: clouds are a special case - we use the results of product 3660 as one way to mark cloudy pixels.

5.8　Data Dependencies

Data dependencies for the MODIS Sea_sfc Temperature proto-algorithm are as follows. This product itself requires Level-1A infrared radiances (product 3708) for bands 20, 22, 23, 31 and 32, and the cloud screening (product 3660). Visible and near infrared radiances (bands 3,4,5,6) will be used as a secondary cloud flag in the event that the cloud screening product is not available. Future versions of this algorithm may use surface wind estimates to better determine the extent of sun-glint and skin- *vs.* bulk-temperature differences during daytime passes. The AIRS SST estimate (product 2523) will be used in near-real time quality assessment of skin temperature. Data dependencies are specified in Table 23. Note that the only products that must be available for Sea_sfc product generation are the Level 1A Radiances (product 3708) and the cloud screening (product 3660).

Table 23. MODIS Sea_sfc Data Dependencies

Instrument	Product	Product #	Band	Necessary
MODIS	Level 1A Radiance	3708	3,4,5,6,20,22,23,31,32*	Yes
Various	Cloud Screening	3660	n/a	Yes
NSCATT-II	Sigma 0	3721	n/a	No
AIRS	SST (Skin)	2523	n/a	No

* Note: Bands 3,4,5,6 are averaged to 1000 m IFOV.

5.9   Output Product

Output retrieved SST estimates for the MODIS Sea_sfc Temperature algorithm are vectors composed of the retrieved SST value, input calibrated radiances, and derived brightness temperatures for each band, flags which quantify the cloud screening results, latitude, longitude and time. There are two products: a quality assessment product for internal use (Table 24) and the Sea_sfc temperature product for external use (Table 25). A description of the vector components and data types is given in Tables 24 and 25.

Table 24. MODIS IR SST Quality Assessment Product

Parameter	Format
SST estimate	32 bit floating point
Latitude	32 bit floating point
Longitude	32 bit floating point
Time	32 bit floating point
Satellite Zenith Angle	32 bit floating point
Solar Zenith Angle	32 bit floating point
Calibrated Radiance - Band 1	32 bit floating point
...	32 bit floating point
Calibrated Radiance - Band n	32 bit floating point
Brightness Temperature - Band 1	32 bit floating point
...	32 bit floating point
Brightness Temperature - Band n	32 bit floating point
Quality Control Flags - 1	16 bit integer
Quality Control Flags - 2	16 bit integer

Table 25. MODIS IR SST Output Product 2527

Parameter	Format
SST estimate	32 bit floating point
Latitude	32 bit floating point
Longitude	32 bit floating point
Time	32 bit floating point
Quality Control Flags - 1	16 bit integer
Quality Control Flags - 2	16 bit integer

These tables provide a basis for estimation of the output data flow for the algorithm. The level 2 output product has a data flow of 3.5 x 10^8 (ocean pixels) x 20 bytes/pixel x 2 fields/day or ~15 Gbytes/day. The data assessment product has a data flow of 3.5 x 10^8 (ocean pixels) x 84 bytes/pixel x 2 fields/day or ~63 Gbytes/day.

6.0 Constraints, Limitations, Assumptions

Major constraints on data quality outside the scope of this effort focus in the following areas: accurate pre-launch instrument characterization, instrument NEΔT for each band, calibration model performance, availability of quality controlled surface calibration-validation observations, availability and access to the various quality assessment data sets, and timely access to continuing performance assessment data sets. The on-orbit instrument NEΔT performance is a primary input to the algorithm error budget. Similarly, a robust calibration model that minimizes radiometer calibration inaccuracies is a necessary requirement for good algorithm performance - this model must limit the non-linear components of such inaccuracies to the least bit count. Surface calibration/validation is also necessary to maintain a regular series of comparison observations to demonstrate system performance. Combination of the surface calibration/validation observations with the quality assessment datasets will permit documentation of system performance and addressing of any anomalies in a timely manner.

7.0 References

Abbott, M.R. and D.B. Chelton, 199l. Advances in passive remote sensing of the ocean. US National Report to IUGG. *Rev. of Geophys., Supplement*: 571-583.

Armitage, S., D. Corney, G. Mason, W. H. Taylor, R. E. J. Watkins, E. J. Williamson, D. Cragg, G. Mellor, D. Tinkler, A. R. Holmes, W. Linford and F. Spry, 1990. Test and calibration of the Along Track Scanning Radiometer (ATSR). Proceedings of the International Symposium on Environmental Testing for Space Programmes - Test, Facilities and Methods. ESA SP-304. 559.

Anding, D. and R. Kauth, 1970. Estimation of Sea Surface Temperature from Space. *Remote Sensing of the Environment*, **1**, 217-220.

Barton, I.J., A.J. Prata, and D.T. Llewellyn-Jones, 1993. The Along Track Scanning Radiometer–an Analysis of coincident ship and satellite measurements, *Adv. Space Res.,* **13(5)**, 69.

Barton, I.J., A.M Závody , D.M. O'Brien, D.R. Cutten, R.W. Saunders and D.T. Llewellyn-Jones, 1989. Theoretical algorithms for satellite-derived sea surface temperatures. *J. Geophys. Res.*, **94**, 3365.

Bradshaw, J.T., H.E. Fuelberg, 1993: An evaluation of HIS interferometer soundings and their use in mesoscale analysis. *J. Appl. Meteor.*, **32**, 522-538.

Bransom, M.A., 1968). *Infrared radiation*, New York, Plenum Press, 623 pp.

Brown, O.B. and R.E. Cheney, 1983. Advances in satellite oceanography. *Rev. Geophys. and Space Phys.,* **21**(5), 1216-1230.

Brown, O.B., J. W. Brown and R.H. Evans, 1985. Calibration of advanced very high resolution radiometer infrared observations. *J. Geophys. Res.*, **90**(C6): 11667-11677.

Casey, K.S. and P. Cornillon, 1999. A comparison of satellite and in situ based sea surface temperature climatologies, *Journal of Climate.* In press.

Cendral, C.J. 1995. Polar Platform for Envisat-1 mission. *Earth Observation Quarterly*, no **49**, p16.

Chahine, M.T., 1980. Infrared remote sensing of sea surface temperature. In *Remote Sensing of Atmospheres and Oceans*, ed. A. Deepak, Academic Press, New York, pp. 411-434.

Clough, S.A., F.X. Kneizys and R.W. Davies, 1989. Line shape and the water vapor continuum. *Atmos. Res.*, **23**, 229-241.

Cornillon, P., and L. Stramma, 1985. The distribution of diurnal sea surface warming events in the western Sargasso Sea. *J. Geophys. Res.*, **98**(C6), 11811-11815.

Craeye, C. and P. Schlussel, 1998. Rainfall on the sea: surface renewals and wave damping. *Boundary-layer meteorology,* **89**, 349.

Cox, C. and W. Munk, 1954. Measurements of the roughness of the sea surface form photographs of the sun's glitter. *J. Op. Soc. Am.*, **44**, 838-850.

d'Almeida, G.A., P. Koepke, and E.P. Shettle, 1991. Atmospheric Aerosols: Global Climatology and Radiative Characteristics, A. Deepak Pub., Hampton, Virginia. 560 pp.

Deschamps, P.Y. and T. Phulpin, 1980. Atmospheric corrections of infrared measurements of sea surface temperature using channels at 3.7 μm, 11 μm and 12 μm. *Boundary Layer Meteor.* **18**, 131-143.

Edwards, T., R. Browning, J. Delderfield, D. J. Lee, K. A. Lidiard, R. S. Milborrow, P. H. McPherson, S. C. Peskett, G. M. Toplis, H. S. Taylor, I. Mason, G. Mason, A. Smith and S. Stringer, 1990. The Along Track Scanning Radiometer - Measurement of sea-surface temperature from ERS-1. *Journal of the British Interplanetary Society*, **43**, 160.

Emery , W., Y. Yu, G. Wick, P. Schluessel and R.W. Reynolds, 1994. Correcting infrared satellite estimates of sea surface temperature for atmospheric water vapor attenuation. *J. Geophys. Res.*, **99**, 5219-5236.

ESSC, 1988. *Earth System Science: A Closer View.* Report of the Earth System Sciences Committee, NASA Advisory Council. Available from Office for Interdisciplinary Earth Studies, University Corporation for Atmospheric Research, Boulder, CO, 208 pp.

Friedman, D., 1969. Infrared characteristics of ocean water (1.5 - 15μm). *Appl. Opt.*, **8**, 2073-2078.

GOFS, 1984. *Global Ocean Flux Study, Proceedings of a Workshop, September 10-14, 1984.* National Academy of Sciences Press, Washington, D.C., 360 pp.

Gross, E.P., 1955. Shape of collision-broadened spectral lines, *Phys. Rev.*, **97**, 395-403.

Harrison, L., J. Michalsky and J. Berndt, 1994. Automated multifilter rotating shadow-band radiometer: an instrument for optical depth and radiation measurements. *Appl. Optics*, **33**, 5118-5125.

Harrison, L. and J. Michalsky, 1994. Objective algorithms for the retrieval of optical depths from ground-based measurements. *Appl. Optics*, **33**, 5126-5132.

Kannenberg, R. 1998. Infrared (IR) instrument comparison workshop at the Rosenstiel School of Marine and Atmospheric Science (RSMAS). The Earth Observer, 1998.

King, M., and D. Herring, 1992. The MODIS Airborne Simulator (MAS). *The Earth Observer*, Nov/Dec 1992.

Kumar, A., P.J. Minnett and R.H. Evans, 1999. AVHRR Pathfinder: algorithm performance. *International Scientific Symposium on Biogeochemistry of the Arabian Sea: Synthesis and Modeling*. Poster presentation.

Lauritson, L., G.J. Nelson and F.W. Porto, 1979. Data extraction and calibration of TIROS-N/NOAA radiometers. NOAA TM NESS 107. US Government Printing Office, Washington, D.C., 81 pp. Available from NTIS.

Llewellyn-Jones, D.T., P.J. Minnett, R.W. Saunders and A.M. Závody , 1984. Satellite multichannel infrared measurements of sea surface temperature of the N.E. Atlantic Ocean using AVHRR/2. *Quart. J. R. Met. Soc.* **110**, 613-631.

Masuda, K., T. Takashima, Y. Takayama, 1988. Emissivity of Pure and Sea Waters for the Model Sea Surface in the Infrared Window Regions. *Remote Sensing of the Environment*, **24**, 313-329.

Mather, J.H., T.P. Ackerman, W. Clements, F. Barnes, M. Ivey, L. Hatfield, and R.M. Reynolds, An Atmospheric Radiation and Cloud Station in the Tropical Western Pacific. *Bull. Amer. Meteor. Soc.*, **78**, 627-642, 1998.

McClain, E.P., 1981. Multiple atmospheric -- window techniques for satellite derived sea surface temperatures. *Oceanography from Space,* **13**, J.F.R. Gower, ed., Plenum, New York.

McClain, E.P., W.G. Pichel, C.C. Walton, Z. Ahmed, and J. Sutton, 1983. Multi-channel improvements to satellite derived global sea surface temperatures. Proc. XXIV COSPAR, *Advances Space Res.* **2**(6), 43-47.

McClain, E.P., W.G. Pichel and C.C. Walton, 1985. Comparative performance of AVHRR-based multichannel sea surface temperatures. *J. Geophys. Res.* **90**(C6), 11587-11601.

Minnett, P.J., 1986. A numerical study of the effects of anomalous North Atlantic atmospheric conditions on the infrared measurement of sea surface temperature from space. *J. Geophys. Res.*, **91**(C7), 8509-8521.

Minnett, P.J., 1990a. Satellite infrared scanning radiometers - AVHRR & ATSR. In *Microwave Remote Sensing for Oceanographic and Marine Weather-Forecast Models,* R.A. Vaughn, ed. Kluwer Academic Publishers.

Minnett, P.J., 1990b. The regional optimization of infrared measurements of sea-surface temperature from space. *J. Geophys. Res.*, **95**, 13,497-13,510.

Minnett, P.J., 1991. Consequences of sea surface temperature variability on the validation and applications of satellite measurements. *J. Geophys. Res.*, **96**, 18,475-18,489

Minnett, P.J., 1995a. Sea surface temperature measurements from the Along-Track Scanning Radiometer on ERS-1. In "Oceanographic Applications of Remote Sensing", M. Ikeda and F. Dobson (eds.). CRC Press Inc. 131-143.

Minnett, P.J., 1995b. The Along-Track Scanning Radiometer: Instrument Details. In "Oceanographic Applications of Remote Sensing", M. Ikeda and F. Dobson (eds.). CRC Press Inc. 461-472.

Mlawer, E.J., S.A. Clough, P.D. Brown and D.C. Tobin, 1998. Collision-induced effects and the water vapor continuum. Eighth Atmospheric Radiation Measurement (ARM) Science Team Meeting, Tucson, AZ. March 1998. US Dept of Energy, Office of Energy Research, Office of Health and Environmental Research, Environmental Sciences Division. pp 503-511.

MODIS, 1986. *MODIS, Moderate-resolution imaging spectrometer, Earth Observing System, IIb.* Instrument Panel Report, National Aeronautics and Space Administration, Washington, D.C., 59 pp.

Nalli, N.R., 1995. Sea surface skin temperature retrieval using the High-Resolution Interferometer Sounder, MS Thesis, University of Wisconsin-Madison. 117pp.

Nalli, N.R. and W.L. Smith, 1998. Improved remote sensing of sea surface skin temperature using a physical retrieval method. *J. Geophys. Res.*, **103,** 10,527-10,542.

Planet, W. (Ed). Data extraction and calibration of TIROS-N/NOAA radiometers. NOAA Tech. Memo. NESS 107- Rev.1. October, 1988.

Podestà, G.P., S.C. Shenoi, J.W. Brown and R.H. Evans, 1990. AVHRR Pathfinder Oceans Matchup database 1985-1994 (Version 18).

Podestà, G.P., S.C. Shenoi, R.H. Evans and O.B. Brown, 1997. Paper in preparation.

Post, M.J., C.W. Fairall, A.B. White, Y. Han, W.L. Ecklund, K.M. Weickmann, D.I. Cooper, P.J. Minnett, P.K. Quinn, S. M. Sekelsky, R.E. McIntosh, and R.O. Knuteson. 1997. The Combined Sensor Program: An air-sea science mission in the central and western Pacific Ocean. *Bull. Am. Met. Soc.*, **78**, 2797-2815.

Prabhakara, C., G. Dalu and V.G. Kunde, 1974. Estimation of Sea Surface Temperature from remote sensing in the 11 μm to 13 μm window region. *J. Geophys. Res.* **79**(12), 1744-1749.

Revercomb, H. E., H. Buijs, H. B. Howell, D. D. Laporte, W. L. Smith, and L. A. Sromovsky, 1988. Radiometric Calibration of IR Fourier Transformation Spectrometers: Solution to a problem with the High-Spectral Resolution Interferometer Sounder. *Appl. Optics*, **27**, 3210-3218.

Reynolds, R. W. and D. C. Marisco, 1993. An improved real-time global sea surface temperature analysis. *J. Climate,* **6**, 114-119.

Robinson, I.S., Wells, N.C. and Charnock, H. 1984. The sea surface thermal boundary layers and its relevance to the measurement of sea surface temperature by airborne and space borne radiometers. *Int. J. Remote Sens.*, Vol. **5**, 19-46.

Rothman, L.S. *et al.*, 1987. The HITRAN database: 1986 edition. *Appl. Opt.*, **26**, 4058-4097.

Rudman, S., R.W. Saunders, C.J. Kilsby and P.J. Minnett, 1994. Water vapour continuum absorption in mid-latitudes: aircraft measurements and model comparisons. *Q. J. R. Met. Soc.*, **120**, 795-807.

Salomonson, V. V., W. L. Barnes, P. W. Maymon, H. E. Montgomery and H. Ostrow, MODIS: Advanced facility instrument for studies of the earth as a system*, IEEE Geosci. Rem. Sens.*, **27**, 145-152, 1989.

Saunders, R.W. and P.J. Minnett, 1990. The measurement of sea surface temperature from the C-130. MRF Internal Note No. 52. Meteorological Research Flight, Royal Aerospace Establishment, Farnborough, Hampshire, U.K., 16pp.

Schluessel, P., H-Y Shin, W.J. Emery and H. Grassl, 1987. Comparison of satellite-derived sea-surface temperature with in-situ skin measurements. *J. Geophys. Res.*, **92**, 2859-2874.

Schluessel, P., W.J. Emery, H. Grassl and T. Mammen, 1990. On the bulk-skin temperature difference and its impact on satellite remote sensing of sea surface temperatures. *J. Geophys. Res.*, **95**, 13,341-13,356.

Schlussel, P., Soloviev, A. V., and W.J. Emery, 1997. Cool and freshwater skin of the ocean during rainfall. *Boundary-layer meteorology*, **82**, 437.

Schmidlin, F.J., 1988. WMO International radiosonde intercomparison phase II, 1985. Instrument and Observing Methods, Report No 29. WMO/TD 312. World Meteorological Organization, Geneva. 113pp.

Schwalb, A., 1973 Modified version of the improved TIROS operational satellite (ITOS D-G). *NOAA TM NESS 35.* Available from NTIS as COM-72-10547. 48 pp.

Schwalb, A., 1978 The TIROSN/NOAA A-G satellite series. *NOAA TM NESS* **95**. Available from NTIS. 75 pp.

Selby, J.E.A., F.X. Kneizys, J.H. Chetwynd Jr., and R.A. McClatchey, 1978. Atmospheric Transmittance/Radiance: Computer Code LOWTRAN 4. *AFGL-TR-78-0053, Environmental Research Papers*, No. **626**. Available from NTIS.

Shenk, W.E. and V.V. Salomonson, 1972. A multispectral technique to determine sea surface temperature using NIMBUS II data. *J. Phys. Oceanogr.* **2**, 157-167.

Smith, A.H., R.W. Saunders and A.M. Závody , 1994. The validation of ATSR using aircraft radiometer data over the Tropical Atlantic. *J. Atmos. and Oceanogr. Techn.* 789-800.

Smith, W.L., R.O. Knuteson, H.E. Revercomb, W. Feltz, H.B. Howell, W.P. Menzel, N.R. Nalli, O. B. Brown, J. Brown, P.J. Minnett and W. McKeown, 1996. Observations of the infrared radiative properties of the ocean - implications for the measurement of sea-surface temperature via satellite remote sensing. *Bull. Am. Met. Soc.*, **77**, 1996, 41-51.

Stokes, G.M. and S.E. Schwartz, 1994. The atmospheric Radiation Measurement (ARM) Program: Programmatic Background and Design of the Cloud and Radiation Test Bed. *Bull. Am. Met. Soc.*, **75**, 1201-1221.

Stramma, L., P. Cornillon, R.A. Weller, J.F. Price and M.G. Briscoe, 1986. Large diurnal sea surface temperature variability: satellite and *in situ* measurements. *J. Phys. Oceanogr.*, **16**, 827-837.

Strong, A.E. and E.P. McClain, 1984. Improved ocean surface temperature from space - comparisons with drifting buoys. *Bull. Am. Meteor. Soc.* **65**(2), 138-142.

Susskind, J., J. Rosenfield, D. Reuter, and M.T. Chahine, 1984. Remote sensing of weather and climate parameters from HIRS2/MSU on TIROS-N. *J. Geophys. Res.*, **89**(C6), 4677-4697.

Walton, C.C., 1988. Nonlinear multichannel algorithms for estimating sea-surface temperature with AVHRR satellite data. *J. Appl. Meteor.* **27**, 115-124.

Walton, C.C., E.P. McClain and J.F. Sapper, 1990. Recent changes in satellite-based multi-channel sea surface temperature algorithms. Preprint, Marine Technology Society Meeting, MTS '90, Washington DC, September 1990.

Watts, P., M. Allen and T. Nightingale, 1996. Sea surface emission and reflection for radiometric measurements made with the along-track scanning radiometer. *J. Atmos. Ocean. Technol.*, **13**, 126-141.

Weller, Robert A. and Peter K. Taylor, 1993. Surface Conditions and Air-Sea Fluxes, CCCO-JSC Ocean Observing System Development Panel, 131 pp. Texas A&M University, College Station, TX 77843-3146.

WOCE, 1985. WOCE Global Air-Sea Interaction Fields, ed. W.G. Large, US *WOCE Technical Report* No. **1**, September 1985, 36 pp.

Wu, X. and W.L. Smith, 1997. Emissivity of rough sea surface for 8-13 μm: modeling and validation. *Applied Optics*, **36**, 1-11

Závody , A.M., C.T. Mutlow, and D.T. Llewellyn-Jones, 1995. A radiative transfer model for sea surface temperature retrieval for the Along-Track Scanning Radiometer, *J. Geophys. Res.*, **100**, 937-952.